Computer Engineering Department
Faculty of Engineering
Deanery of Higher Studies
Islamic University – Gaza
Palestine

Enhancing Iris Recognition

By

Shaaban A. Sahmoud

Supervisor

Prof. Ibrahim S. I. Abuhaiba

A Thesis Submitted in Partial Fulfillment of the Requirements for the Degree of Master of Science in Computer Engineering

1432H (2011)

بسم الله الرحمن الرحيم

الجامعة الإسلامية – غزة
The Islamic University - Gaza
عمادة الدراسات العليا
هاتف داخلي: 1150

الرقم Ref ج س غ/35/
2011/09/26
التاريخ Date

نتيجة الحكم على أطروحة ماجستير

بناءً على موافقة عمادة الدراسات العليا بالجامعة الإسلامية بغزة على تشكيل لجنة الحكم على أطروحة الباحث/ **شعبان أحمد إبراهيم سهمود** لنيل درجة الماجستير في **كلية *الهندسة*** **قسم هندسة الحاسوب** وموضوعها:

Enhancing Iris Recognition

وبعد المناقشة التي تمت اليوم الثلاثاء 29 شوّال 1432هـ، الموافق 2011/09/27م الساعة الحادية عشرة صباحًا، اجتمعت لجنة الحكم على الأطروحة والمكونة من:

أ.د. إبراهيم سليمان أبو هيبة	**مشرفاً ورئيساً**	.....
د. أيمن أحمد أبو سمرة	**مناقشاً داخلياً**	.....
د. وسام محمود عاشور	**مناقشاً داخلياً**	.....

وبعد المداولة أوصت اللجنة بمنح الباحث درجة الماجستير في **كلية *الهندسة*** / قسم **هندسة الحاسوب.**

واللجنة إذ تمنحه هذه الدرجة فإنها توصيه بتقوى الله ولزوم طاعته وأن يسخر علمه في خدمة دينه ووطنه.

والله ولي التوفيق،،،

عميد الدراسات العليا

أ.د. فؤاد علي العاجز

Acknowledgment

First of all I would like to said Praise be to Allah for everything and for giving me the power and help to accomplish this research and making this work successful.

This thesis would have been an impossible task without the assistance, support, valuable advice and encouragement of my supervisor Prof. Ibrahim S. I. Abuhaiba.

I also thank my wife, Abeer, for staying up late with me when I have had deadlines to meet, and for being my number one fan.

Finally I would like to thank all my family members who have been constant source of motivation, inspiration and support during my whole educational life and also their guidance.

Contents

List of Abbreviations

HD	Hamming Distance
FAR	False Accept Rate
FRR	False Reject Rate
CAR	Correct Accept Rate
CRR	Correct Reject Rate
FMR	False Match Rate
FNMR	False Non Match Rate
CMC	Cumulative Match Characteristic
TP	True Positive
TN	True Negative
TA	True Accept
TR	True Reject
EER	Equal Error Rate
ROC	Receiver Operating Characteristic
CHT	Circular Hough Transform
NIR	Near Infrared
CASIA	Chinese Academy of Sciences Institute of Automation

List of Tables

List of Figures

تحسين التعرف على قزحية العين

شعبان أحمد سهمود

ملخص

في هذه الرسالة نعرض ثلاث طرق لزيادة دقة خوارزميات تحديد هوية الإنسان باستخدام بصمة قزحية العين. أولا نعرض خوارزمية تقوم بتقسيم الصورة وتحديد مكان القزحية وحدودها عندما تستخدم صور للعين التقطت في ظروف غير مثالية. هذه الخوارزمية تقوم بتقليل الأخطاء الناتجة عن استخدام صور في ظروف غير مثالية مثل انعكاسات الضوء على العين وتغطية الرموش والجفون لأجزاء من العين. ستبدأ الخوارزمية بتحديد المنطقة على الصورة المتوقع وجود القزحية فيها باستخدام خوارزمية (K-means) ومن ثم سيتم تحديد حدود قزحية العين باستخدام طريقة مشهورة اسمها (Circular Hough Transform) وأخيرا سنقوم بتحديد وعزل المناطق التي تضررت أو تم تغطيتها على قزحية العين بسبب الضوء أو الجفون أو الرموش.

ثانيا ندرس مشكلة تمدد بؤرة العين السوداء و نثبت مدى تأثيرها على أداء و دقة نظام تحديد الهوية باستخدام بصمة قزحية العين. ومن ثم نقوم عمليا بتحديد الحد الأقصى المسموح لبؤرة العين أن تتمدد إليه بحيث إذا تجاوز التمدد هذا الحد سينتج عنه أخطاء أو أضرار على دقة البصمة.

أخيرا قمنا بتحليل قطاع البصمة كل ثنائية على حدة لتحديد أي منها أكثر استقرار من الآخر و لمعرفة المناطق الأكثر أهمية للتركيز عليها في الحصول على بصمة العين.

لتقييم الخوارزميات التي قمنا بتطويرها استخدمنا ثلاث أنواع لقواعد بيانات قزحية العين و هي عامة ومتوفرة على الانترنت مجانا. كل الخوارزميات التي قمنا بتطويرها تم برمجتها باستخدام برنامج MATLAB 7.0. أما الحاسوب الذي أجرينا باستخدامه التجارب فكانت مواصفاته كما يلي: نوع الحاسوب هو Compaq . نوع وسرعة المعالج هي Core 2 Due Intel Pentium (2.00 GHz) وسعة الذاكرة هي 1GB . أما نظام التشغيل المستخدم فهو Windows 7. في التجربة الأولى استخدمنا قاعدة بيانات تسمى (UBIRIS v1) لتقييم خوارزمية التقسيم وكانت الدقة الناتجة تساوي 98.76% وهي ممتازة مقارنة بالطرق الأخرى. أما وقت التنفيذ فكان يساوي 1.68 ميلي ثانية وهو أقل من الوقت المستنفذ في الطرق الأخرى. ولتقييم خوارزمية تمدد بؤرة العين استخدمنا قاعدة بيانات للصور تسمى (CASIA v3) وأثبتت النتائج حصول تحسن كبير في الأداء بعد استثناء العيون التي تمدد بؤرتها أكبر من الحد الذي قمنا بتحديده عمليا. وأخيرا استخدمنا (CASIA v4) لإثبات وجود مجموعة من الثنائيات الغير مستقرة في قطاع بصمة العين. وقمنا بعد ذلك بدراسة أي المقاطع تحتوي على عدد أكبر من الثنائيات الغير مستقرة , وقد أثبتت النتائج أن القطاعات الداخلية للعين أفضل من القطاعات الخارجية. النتائج التي حصلنا عليها تؤكد أن الخوارزميات التي قمنا بتطويرها زادت من دقة بصمة قزحية العين وبالتالي ستساعد على تجاوز مشكلات التقسيم وتمدد بؤرة العين مما يمكننا من استخدام بصمة قزحية العين في ظروف أكثر سهولة وغير مثالية. وهذا سيؤدي إلى انتشار أوسع لاستخدامات بصمة قزحية العين.

Enhancing Iris Recognition

Shaaban A. Sahmoud

Abstract

In this thesis, we propose three techniques to increase the iris recognition robustness and accuracy. First, we propose a new segmentation algorithm to handle iris images were captured on less constrained conditions. This algorithm reduces the error percentage while there are types of noise, such as iris obstructions and specular reflection. The proposed algorithm starts by determining the expected region of iris using K-means clustering algorithm, then circular Hough transform is used to localize iris boundary. After that, some proposed algorithms will be applied to detect and isolate noise regions.

Second, a study of the effect of the pupil dilation on iris recognition system is performed, in order to show that the pupil dilation degrades iris template and affects the performance of recognition systems. Therefore, a limit of pupil dilation degree is determined. If the degree of pupil dilation exceeds this limit, the iris code will be affected or some of its information will be discarded. This limit can be used to avoid detrimental pupil dilation.

Finally, we analyze the iris code bits to determine the consistent and inconsistent bits, and we compare between the inner and outer regions to find which region contains more inconsistent bits.

In our experiments, we use three free public iris' databases (UBIRIS v1, CASIA v3 and CASIA v4). Each of our algorithms were implemented in the MATLAB 7.0 software. The environment where the experiments are performed in is Compaq PC, Core 2 Due Intel Pentium Processor (2.00 GHz), 1GB RAM and Windows 7 operating system. Experiments on UBIRIS v1 show that the accuracy of our segmentation algorithm is 98.76%, which significantly improves the performance of iris recognition, and the average execution time of our segmentation algorithm equals 1.68 ms, which is less than the execution time of the other algorithms. Experiments on CASIA v3 show that the effect of pupil dilation can be minimized significantly by excluding irises which have a pupil dilation degrees more than the estimated limit of dilation degree. Finally, experiments on CASIA v4 show the existence of inconsistent bits in the iris code, and also show that the bits of inner regions are more stable than the bits of outer regions. Results show that this work significantly improve the performance of iris recognition, and make it possible to be applied in wide environments, especially in non-cooperative environments.

Keywords: Iris Recognition, Iris Segmentation, Non-Cooperative Iris Recognition, K-means Clustering, Circular Hough Transform, Pupil Dilation, Inconsistent Bits, Iris Code Analysis.

Chapter 1

Introduction

With an increasing emphasis on security, the need for automated personal identification system based on biometrics has increased. This is because traditional identification systems based on cards or passwords can be broken by losing or stealing cards and forgetting passwords. So, there is a need for identification systems identify humans without depending on what person possesses or what person remembers. Biometrics [1, 2] can be divided into two main classes: physiological and behavioral. The physiological class is related to the shape of the body including fingerprint, face recognition, DNA, palm print, hand geometry, and iris recognition. The behavioral class is related to the behavior of a person and includes typing rhythm, gait, and voice.

Recently, iris recognition is becoming one of the most important biometrics used in recognition when imaging can be done at distances of less than two meters. This importance is due to its high reliability for personal identification [3, 4, 5]. Human iris has great mathematical advantage that its pattern variability among different persons is enormous [6], because iris patterns possess a high degree of randomness. In addition, iris is very stable over time [7, 8]. Since the concept of automated iris recognition was proposed in 1987 [7], many researchers worked in this rang and proposed many powerful algorithms. These algorithms were based on the texture variations of the iris and can be divided into many approaches [9], phase-based methods [3, 10, 11], zero-crossing representation [12], texture analysis [13, 14], and intensity variations [15]. The most relevant algorithms and widely used in current real applications are the algorithms developed by Daugman.

There are many commercial iris capture systems capture images of the iris using near-infrared illumination, such as the LG 2200 and LG 4000. Most systems in use today need explicit user cooperation, requiring that the user is positioned correctly to acquire a high-quality image. These systems provide auditory feedback to the user to ensure that they are properly positioned for image acquisition. In the United Kingdom, the Iris Recognition Immigration System (IRIS) is a voluntary system that allows travelers to pass through

border control stations at several airports quickly, validating their identify using automated “barriers”. CANPASS in Canada is a similar program to allow frequent travelers to quickly move through security checkpoints at airports.

1.1 Contributions

This research aims to improve the performance of iris recognition by solving some problems that cause errors in iris recognition system. The main contributions of this thesis include:

- The proposal of a more robust iris segmentation method able to deal with highly noisy iris images capturing on less constrained conditions and non-ideal environments. In this method K-means clustering, Canny edge detection, circular Hough transform, and some new proposed algorithms are used to deal with expected types of noise. This segmentation algorithm reduces the error percentage, when there are types of noise, such as: iris obstructions and specular reflection.

- The study and discussion of pupil dilation problem and its effects on iris recognition system. Then the maximum allowable limit of pupil dilation degree is experimentally estimated. Therefore, no iris should exceeds this limit to prevent the recognition system from errors occurrence.

- The analysis of the bits of iris' template to investigate the existence of inconsistent bits in iris template, and to find regions that contain more of inconsistent bits than the other regions. This analysis can be used to avoid inconsistent regions that contain large number of inconsistent bits in order to improve the performance of iris recognition systems.

1.2 Biometrics

Biometrics consist of methods for uniquely recognizing humans based upon one or more intrinsic physical or behavioral traits [16]. Another definition defines biometrics as the science and technology of measuring and analyzing biological data. In information

technology, biometrics refers to technologies that measure and analyze human body characteristics, such as fingerprints, eye retinas and irises, voice patterns, facial patterns and hand measurements, for authentication purposes [17]. Biometrics can be divided to two main classes

- Physiological: are related to the shape of the body. Examples include, but are not limited to fingerprint, face recognition, DNA, palm print, hand geometry, iris recognition, which has largely replaced retina, and scent.

- Behavioral: are related to the behavior of a person. Examples include, but are not limited to typing rhythm, gait, and voice. Some researchers have coined the term behaviometrics for this class of biometrics.

Voice sometimes can be a physiological trait because every person has a different vocal tract, but voice recognition is mainly based on the study of the way a person speaks, commonly classified as behavioral.

It is possible to understand if a human characteristics can be used for biometrics in terms of the following parameters [18]:

- Universality – each person should have the characteristic.
- Uniqueness – is how well the biometric separates individuals one from another.
- Permanence – measures how well a biometric resists aging and other variance over time.
- Collectability – ease of acquisition for measurement.
- Performance – accuracy, speed, and robustness of technology used.
- Acceptability – degree of approval of a technology.
- Circumvention – ease of use of a substitute.

The first time an individual uses a biometric system is called an enrollment. During the enrollment, biometric information from an individual is stored. In subsequent uses, biometric information is detected and compared with the information stored at the time of enrollment. Note that it is crucial that storage and retrieval of such systems themselves be secure if the biometric system is to be robust.

Figure 1.1 illustrates the basic block diagram of a biometric system. The first block (sensor) is the interface between the real world and the system; it has to acquire all the necessary data. Most of the times it is an image acquisition system, but it can change according to the characteristics desired. The second block performs all the necessary pre-processing: it has to remove artifacts from the sensor, to enhance the input (e.g. removing

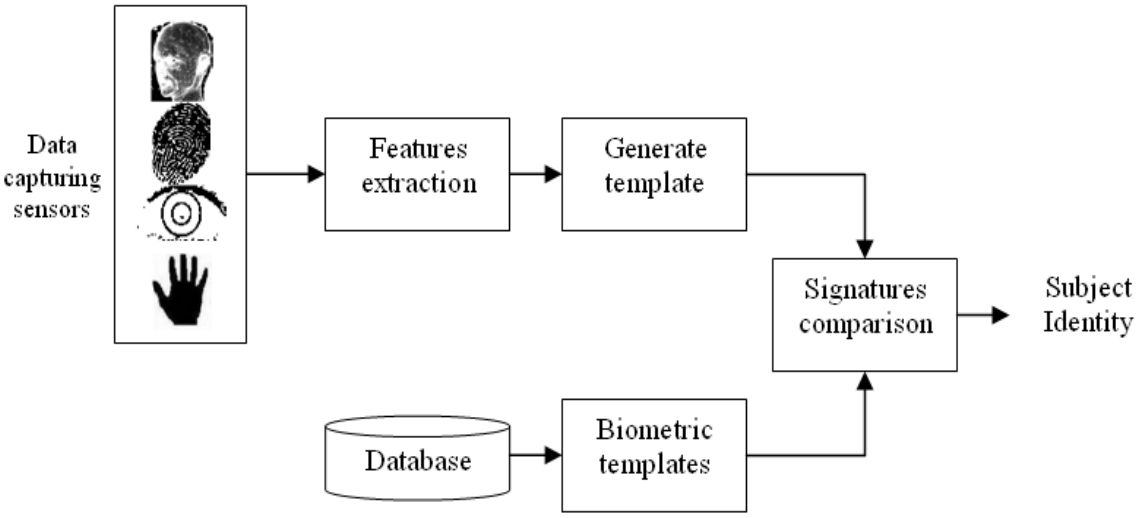

Figure 1.1: The basic block diagram of the biometric system.

background noise), to use some kind of normalization, etc. and finally necessary features are extracted. The last step is an important step as the correct features need to be extracted in the optimal way. A vector of numbers or an image with particular properties is used to create a template. A template is a synthesis of the relevant characteristics extracted from the source. Elements of the biometric measurement that are not used in the comparison algorithm are discarded in the template to reduce the file size and to protect the identity of the enrollee. If enrollment is being performed, the template is simply stored somewhere (on a card or within a database or both). If a matching phase is being performed, the obtained template is passed to a matcher that compares it with other existing templates, estimating the distance between them using any algorithm (e.g. Hamming distance). If the distance between them is less than specified threshold value, the two compared templates will assumed to be matched and vice versa. The most common biometrics [19] that are presently used for security purposes are:-

DNA

The deoxyribonucleic acid (DNA) is represented through a one-dimensional code, unique for each person. The only exception are identical twins, which can represent a serious problem, regarding security and forensic applications [20]. This method is considered to have some drawbacks, as the easy contamination and sensitivity, the impossibility to perform real-time recognition and severe privacy issues, due to the DNA can reveal susceptibility to some diseases.

Face

Facial images are the most common biometric characteristic used by humans to perform personal recognition. This is a non intrusive and suitable trait to perform covert recognition. Three types of feature extraction methods can be distinguished: generic methods based on edges, lines, and curves; feature-template-based methods that are used to detect facial features such as eyes and structural matching methods that take into consideration geometrical constraints on the features [21]. Although performance of commercially available systems is reasonable, there is still significant room for improvement, since false rejection rate is about 10% and the false accept rate is about 1% [22]. These systems face strong difficulties when the faces are captured under different angles and uncontrolled ambient illumination.

Fingerprint

Used for many centuries, either by creating an ink impression of its patterns or using a reader device, the access to the details of fingerprint ridges and furrows, allied to some minutiae points, can determine its uniqueness. Although being a mature and easy-to-use technology, it also requires user cooperation and is vulnerable to noise.

Gait

Although it was originally performed through the use of physical devices attached to the subjects' legs, the vision-based gait biometrics has recently received a lot of attention, and the first known effort towards recognition was made by Niyogi and Adelson in the early 1990s [23]. The human gait is a periodic activity with each gait cycle covering two

strides: the left foot forward and right foot forward strides. Each stride spans the double-support stance to the legs-together stance as the legs swing past each other and back to the double-support stance. Gait vulnerability to changes in the walking surface, walking speed or in the carrying conditions were reported. Due to these, gait-based biometric systems tend to present high false rejection rates. Also, since video-sequence is used to capture the required data, it is considered as one of the most computationally expensive methods.

Iris

The iris is a complex pattern which contains many distinctive features such as arching ligaments, furrows, ridges, crypts, rings, corona, freckles and a zigzag collarette. Each iris is unique and even irises of identical twins are different. Furthermore, the iris is more easily imaged than retina; it is extremely difficult to surgically tamper iris texture information and it is possible to detect artificial irises. Although the early iris based identification systems required considerable user participation and were expensive, efforts are underway to build more user-friendly and cost-effective versions. To obtain a good image of the iris, identification systems typically illuminate the iris with near-infrared light, which can be observed by most cameras yet is not detectable by humans. The available results of both accuracy and speed of iris-based identification are highly encouraging and point to the feasibility of large-scale recognition using iris information. Due to this and to the above described characteristics, it is common to consider iris as one of the best biometric traits, although this evaluation is dependent on the specific purpose.

Keystroke

The behavioral biometric of Keystroke Dynamics uses the manner and rhythm in which an individual types characters on a keyboard or keypad. The keystroke rhythms of a user are measured to develop a unique biometric template of the users typing pattern for future authentication. Raw measurements available from most every keyboard can be recorded to determine Dwell time (the time a key pressed) and Flight time (the time between “key up” and the next “key down”). The recorded keystroke timing data is then processed to determine a primary pattern for future comparison. Similarly, vibration information may

be used to create a pattern for future use in both identification and authentication tasks. Oppositely to other traits, the keystroke information can be continuously analyzed by the recognition system, decreasing the probability of active counterfeit measures. Moreover, since users are accustomed to authenticating themselves through usernames and password, most keystroke biometric methods are completely transparent and are well accepted by users. Among potential disadvantages, privacy concerns must be considered, as the way a subject strokes can be used to infer information about its potential rentability and work effectiveness [24].

1.3 Performance of Biometrics

A biometric system can operate in two modes, verification and identification. The next two subsections describe these modes, and how can we evaluate their performance.

1.3.1 Verification

Verification : It is one to one comparison of a captured biometric with a stored template to verify that the individual is the one who he claims to be. If the two samples match well enough, the identity claim is verified, and if the two samples do not match well enough, the claim is rejected. Verification can be done accompanied with a smart card, username or ID number.

In a verification decision context there are four possible outcomes normally called :-

1. **F**alse **A**ccept **R**ate (FAR) or **F**alse **M**atch **R**ate (FMR) or **F**alse **P**ositive (FP):
    - Occurs when the system accepts an identity claim, but the claim is not true.
    - The proportion of impostor attempts whose **H**amming **D**istance (HD) is below a given threshold.
2. **C**orrect **A**ccept (CAR) or **T**rue **P**ositive (TP) or **T**rue **A**ccept (TA):
    - Occurs when the system accepts, or verifies, an identity claim, and the claim is true.

3. **F**alse **R**eject (FRR) or **F**alse **N**on **M**atch **R**ate (FNMR) or **F**alse **N**egative (FN):
    - Occurs when the system rejects an identity claim, but the claim is true.
    - The proportion of genuine or authentic attempts whose HD exceeds a given threshold.
4. **C**orrect **R**eject (CRR) or **T**rue **N**egative (TN) or **T**rue **R**eject (TR):
    - Occurs when the system rejects an identity claim and the claim is false.

Biometric performance in a verification scenario is often summarized in a **R**eceiver **O**perating **C**haracteristic (ROC) curve. The ROC curve plots the verification rate on the Y axis and the false accept rate on the X axis, or, alternatively, the false reject rate on the Y axis and the false accept rate on the X axis. The **E**qual **E**rror **R**ate (EER) is a single number often quoted from the ROC curve. Equal error rates (EER): points at which FMR and FNMR are nearest equal. Equal error rates enable evaluation of FMR and FNMR at a single operating point.

1.3.2 Identification

Identification : It is one to many comparison of the captured biometric against a biometric database or gallery (The set of enrolled samples is often called a gallery) in attempt to identify an unknown individual. The identification only succeeds in identifying the individual if the comparison of the biometric sample with a template in the database falls within a previously set threshold.

As verification mode, in identification decision context there are four possible outcomes normally called like verification :-

1. False Accept Rate (FAR) or False Match Rate (FMR) or False Positive (FP):
    - Occurs when the system says that an unknown sample matches a particular person in the gallery and the match is not correct.
    - The rate at which a matching algorithm incorrectly determines that an impostor’s biometric sample matches an enrolled sample.
    - The proportion of impostor attempts whose HD is below a given threshold.

2. Correct Accept (CA) or True Positive (TP) or True Accept (TA):
    - Occurs when the system says that an unknown sample matches a particular person in the gallery and the match is correct.
3. False Reject (FR) or False Non Match Rate (FNMR) or False Negative (FN):
    - Occurs when the system says that the sample does not match any of the entries in the gallery, but the sample in fact does belong to someone in the gallery.
    - The proportion of genuine or authentic attempts whose HD exceeds a given threshold.
    - The rate at which a matching algorithm incorrectly fails to determine that a genuine sample matches an enrolled sample.
4. Correct Reject (CR) or True Negative (TN) or True Reject (TR):
    - Occurs when the system says that the sample does not match any of the entries in the gallery, and the sample in fact does not.

Performance in an identification scenario is often summarized in a **C**umulative **M**atch **C**haracteristic (CMC) curve. The CMC curve plots the percent of probes correctly recognized on the Y axis and the cumulative rank considered as a correct match on the X axis.

Obviously, the first and third outcomes in the two modes verification and identification are errors, while the second and fourth outcomes are the ones sought. By manipulating the decision criteria, the relative probabilities of these four outcomes can be adjusted in a way that reflects their associated costs and benefits. These values importance may be very different in different applications. In a customer context the cost of a FRR error may exceeds the cost of a FAR error, whereas just the opposite may be true in a military context.

Figure 1.2 illustrates the idea of the decision landscape. The two distributions represent the two states of the world, which are imperfectly separated. The abscissa is any metric of similarity or dissimilarity; in this case it happens to be Hamming Distance, which is the fraction of bits that differ between two binary strings. A decision about whether they are

instances of the same pattern or completely different patterns, is made by imposing some decision criterion for similarity as indicated by the dotted line. Similarity up to some Hamming Distance (0.4 in this case) is deemed sufficient for regarding the patterns as the same, but beyond that point, the patterns are declared to be different.

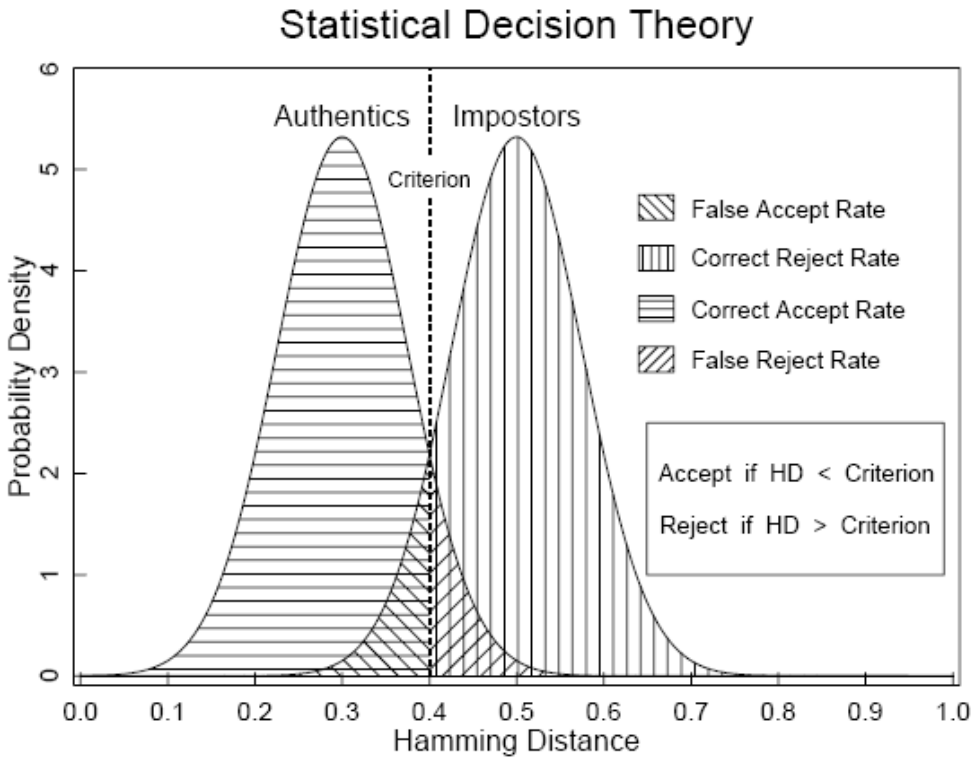

Figure 1.2: Decision landscape: general formalism for biometric decision making [47].

1.4 Iris Anatomy

The iris consists of a pigmented fibrovascular tissue, known as stroma. The stroma connects a sphincter muscle and a set of dilator muscles to open it. It is divided into two major regions: the pupillary and the ciliary zone (Iris). The pupillary zone is the inner portion of the iris whose edges form the pupillary iris border. The ciliary zone is the outer portion of the iris, which extends itself into the iris origin in the ciliary body. The region that separates the pupillary and scleric portions is designated as the collarette. This is typically the region where the sphincter and dilator muscles overlap [19]. Figure 1.3 shows an example image from UBIRIS iris database and regions of each part of the iris.

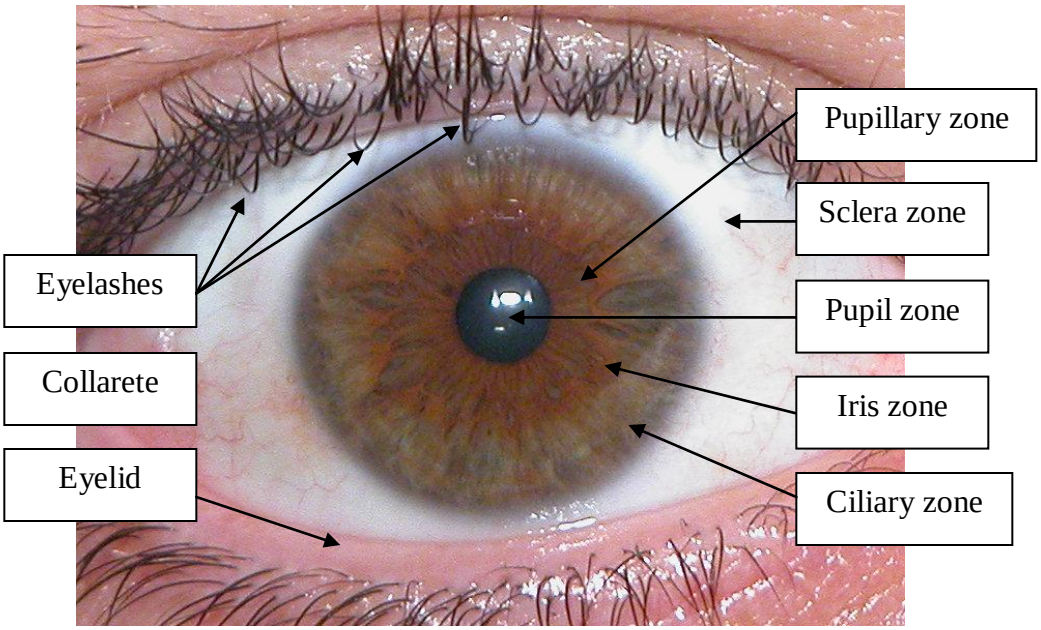

Figure 1.3: Morphology of the human iris (UBIRIS Database).

The iris begins to form during the third month of gestation and the structure is complete by the eight month, although pigmentation continues into the first year after birth [25]. The visible features of the iris arise in the trabeculum, which is a meshwork of connective tissues with arching ligaments, crypts, contraction furrows, a corona and pupillary frill, coloration and freckles. Although the anterior layer covering the trabecular framework creates the predominant iris texture seen with visible light, additional discriminating information can be given by the location of all of these sources of radial and angular variation. Together, as mentioned by Daugman [26], they provide a distinguishable and unique signal.

The texture and minutia of the iris is believed to have high random morphogenesis and no genetic penetrance in its expression. Since the appearance of each iris depends of the initial conditions in the embryonic mesoderm from which it develops, the phenotypic of two iris with the same genetic genotype (e.g., identical twins or the both eyes of a subject) have distinguishable minutia. Past studies about the iris texture concluded that the inter-subject variability of its pattern spans about 250 degrees-of-freedom and have an entropy of about 3.2 bits per square-millimeter. These biological characteristics and the

chaotic appearance of the iris patterns turned it as one of the most suitable traits for biometric purposes. Iris is generally accepted as one of the most promising biometric traits and is the subject for the development and proposal of many biometric recognition algorithms [19].

1.5 Thesis Outline

The rest of our thesis will be as follow, Chapter two introduces the literature review of the four topics 1- the common iris recognition methods, 2- iris segmentation methods, 3- pupil dilation problem solutions, and 4- previous researches in analyzing iris code bits. Chapter three views the background of the techniques we used to develop our proposed iris recognition system. In this chapter, circular Hough transform, K-means clustering algorithms, Canny edge detection algorithm and morphological operations are explained. In Chapter four, the new algorithms will be proposed. First, a new effective and fast iris segmentation algorithm to segment non-ideal iris images is proposed, then a method to avoid the dilation of pupil will be viewed. Finally, the regions of inconsistent bits in iris templates are determined. Chapter five will describe the common public and freely available iris image databases that will be used in this thesis. Then the selected and used datasets in our experiments will be viewed. Then the results of these experiments will be shown and discussed. Finally, Chapter six gives the conclusion and recommendations for future researches.

Chapter 2

Literature Review

In this chapter, we overview the most common iris recognition methods. After that we review the common segmentation methods used in iris recognition. Finally, the previous research in pupil dilation and analyzing iris code are described.

2.1 Iris Recognition Methods

Although there are many proposed iris recognition systems, all of them approximately share the following main stages: iris Segmentation, iris normalization, feature extraction, and feature comparison, as shown in Figure 2.1. In this section, we explain in details the stages of the most common methods in iris recognition system.

2.1.1 Daugman's Method

Daugman's 1994 patent [22] described an operational iris recognition system in some detail. In 2004 his new paper [2] said that image acquisition should use near-infrared illumination so that the illumination could be controlled.

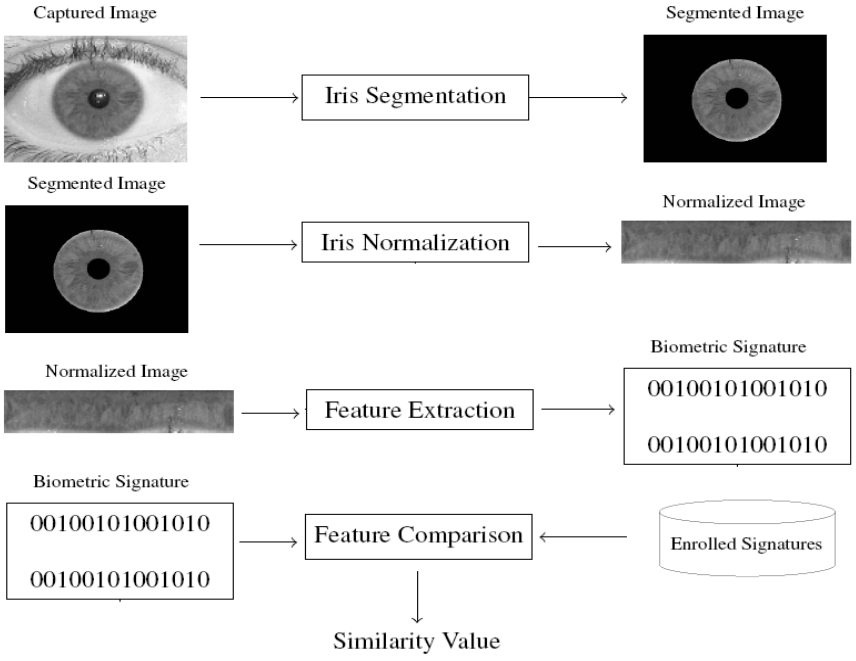

Figure 2.1: Main stages of the iris recognition systems.

Near-infrared illumination also helps reveal the detailed structure of heavily pigmented (dark) irises. the next step is localizing the iris from image. Daugman's approximated the pupil and iris boundaries of the eye as circles. So, he proposed an Integro-Differential operator for detecting the iris boundary by searching the parameter space. Because not all images of an iris are in the same size (e.g. The distance from the camera affects the size of the iris in the image, illumination variations and angle of the image capturing), Daugman proposed the rubber sheet model to normalize the segmented iris. This model representing the iris using a fixed parameter interval in a doubly dimensionless pseudo polar coordinate system. The iris is remapped from raw Cartesian coordinates *(x,y)* to the dimensionless polar coordinate system, which consists of pairs of real coordinates *(r,θ)*, where *r* is in the unit interval [0,1] and θ is an angle in [0,2Π]. This makes all irises have the same size and also simplifies subsequent processing.

To extract the features from the normalized iris Daugman applied a two dimensional texture filter called Gabor filter [27] to an image of the iris and extracted a representation of the texture, called the iris code.

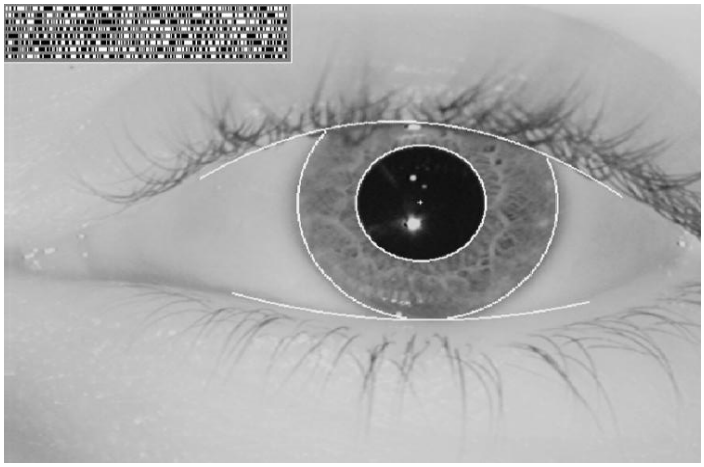

Figure 2.2: Example of an iris with its iris code [6].

The iris code is a set of bits, each one of which indicates whether a given bandpass texture filter (Gabor filter in Daugman algorithm) applied at a given point on the iris image has a negative or nonnegative result. Figure 2.2 shows example of iris code. To compare two iris templates Daugman used Hamming distance as the similarity measure

for two iris signatures. Given two binary sets, *A* and *B*, with *N* bits each: where $A = \{a_1, ..., a_N\}$ and $B = \{b_1, ..., b_N\}$, the Hamming distance is:

$$HD(A,B) = \frac{1}{N} * \sum_{i=1}^{N} a_i \otimes b_i \quad \text{..... (2.1)}$$

where $\otimes$ is the logical XOR operation. Thus, for two completely equal signatures the value of the Hamming distance will be zero, and in completely different signatures, the value of the Hamming distance will be one.

2.1.2 Wildes' Method

Wildes [30] described an iris biometrics system uses different techniques from that of Daugman. To accomplish iris segmentation Wildes used a gradient based binary edge-map construction followed by circular Hough transform. This method became the most common method in iris segmentation, many researchers [31-34] later proposed new algorithms depend on this method.

Wildes applied a Laplacian of Gaussian filter at multiple scales to produce a template and compute the normalized correlation as a similarity measure after normalizing the segmented iris. He used an image registration technique to compensate scaling and rotation then an isotropic band-pass decomposition is proposed, derived from application of Laplacian of Gaussian filters to the image data. In the Comparison stage a procedure based on the normalized correlation between both iris signatures is used.

Although Daugman's system is simpler than Wildes' system, Wildes' system has a less-intrusive light source designed to eliminate specular reflections. Wildes' approach is expected to be more stable to noise perturbations, it makes less use of available data, due to binary edge abstraction, and therefore might be less sensitive to some details. Also, Wildes' approach encompassed eyelid detection and localization [28].

2.1.3 Key Local Variations Method

Li Ma, Tieniu Tan, Yunhong Wang, and Dexin Zhang proposed a new algorithm for iris recognition by characterizing key local variations. The basic idea is that local sharp variation points, denoting the appearing or vanishing of an important image structure, are utilized to represent the characteristics of the iris. First, the background in the iris image is removed by localizing the iris by roughly determine the iris region in the original image, and then use edge detection and Hough transform to exactly compute the parameters of the two circles in the determined region. In order to achieve invariance to translation and scale, the annular iris region is normalized to a rectangular block of a fixed size using the methods in [35, 36]. Then lighting correction and image enhancement is applied to handle the low contrast and non-uniform brightness caused by the position of light sources. Figure 2.3 shows the stages of segmentation and normalization.

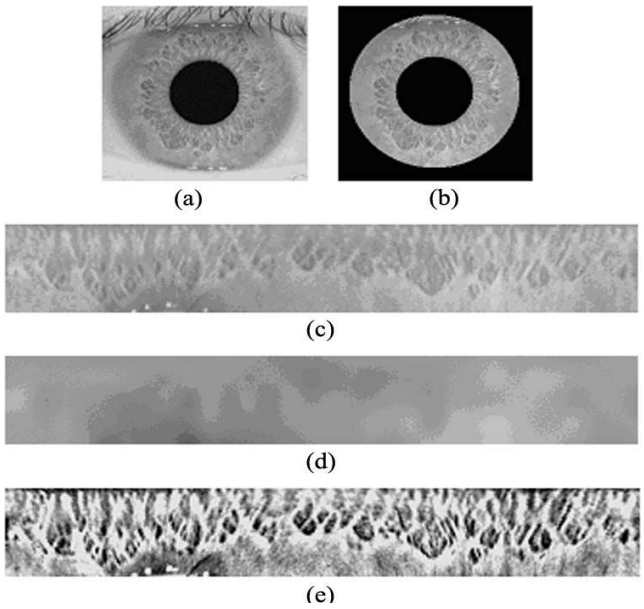

Figure 2.3: Iris image preprocessing: (a) original image. (b) localized image. (c) normalized image; (d) estimated local average intensity. (e) enhanced image [29].

In feature extraction stage they constructed a set of 1-D intensity signals containing the main intensity variations of the original iris for subsequent feature extraction. Using wavelet analysis, they recorded the position of local sharp variation points in each

intensity signal as features. Directly matching a pair of position sequences is also very time-consuming. So, they adopted a fast matching scheme based on the exclusive OR operation to solve this problem [29].

2.2 Segmentation Methods

Many researchers have contributed much in iris segmentation. They have used different techniques to increase the performance of their algorithms. We can classify the previous algorithms into two classifications. First classification according to the region of starting in segmentation, and second classification according to the operators or techniques used to describe the shapes in all eyes.

The Classification According to The Region of Starting.

There are three categories of researchers depending on where do they start the segmentation. The first category of researchers starts from pupil [37, 38] because it is the darkest region in the image. Based on this, pupil is localized and the pupillary boundary of iris is fixed, then the iris is determined using different techniques. Finally, noises are detected and isolated from the iris region.

In the second category, [39] the process starts from the sclera region because the sclera part is found to be less saturated (white) than other parts of the images especially for images containing heavily pigmented (dark) irises, or images affected by noise. After determining the sclera region, the iris is detected using any type of operators. Finally, the pupil and noises are detected and isolated from iris region.

The third category [40, 41] of researchers directly search the iris region using edge operators or apply clustering algorithms to extract texture features of the iris.

Classification According to The Techniques Used to Describe The Shapes in Eyes.

There are two common approaches to localize the iris region according to the used techniques. The first technique [42, 43] is applying type of edge detection followed by Hough transform or one of its derivatives to detect the shape of iris and pupil, sometimes a final stage is applied to correct the shape of iris or pupil.

The second type [37, 44-46] uses different types of operators to detect the edges of iris like Daugman's [23] Integro-Differential operator or Camus and Wildes [48] operator and use the same operator or another one to remove the pupil region.

In the next subsections, we will explain the most famous and robust segmentation methods due to their relevance in the literature.

2.2.1 Daugman's Method

Daugman's method [1] is the most cited in the iris segmentation literature. Iridian Technologies turned it into the basis of 99.5% of the commercial iris recognition systems. It was proposed in 1993 and was the first method effectively implemented in a working biometric system. The author assumes both pupil and iris with circular form and applies the following operator

$$max_{r,x_0,y_0} \left| G_\sigma(r) * \frac{\delta}{\delta r} \oint_{r,x_0,y_0} \frac{I(x,y)}{2\pi r} ds \right| \quad \text{..... (2.2)}$$

Where *I(x,y)* is an image; the operator searches over the image domain *(x,y)* for the maximum in the blurred partial derivative with respect to increasing radius r , of the normalized contour integral *I(x,y)* along a circular arc *ds* of radius *r* and center coordinates (x_0, y_0). The symbol * denotes convolution and $G_\sigma(r)$ is a smoothing function such as a Gaussian of scale δ .This process works very effective on images with enough separability between iris, pupil and sclera intensity values. However, it frequently fails when the images do not have sufficient intensity separability, specially between the iris and the sclera regions. This algorithm can also fail where there are exist types of noise in the eye image, such as reflections. So, it works excellent only on images picked at Near Infrared camera and in ideal imaging conditions.

2.2.2 Camus and Wildes' Method

Camus and Wildes [2] presented a robust, real-time algorithm for localizing the iris and pupil boundaries of an eye in a close-up image. It uses a multi-resolution approach to detect the boundary contours of interest quickly and reliably, even in cases of very low contrast, specular reflections and oblique views. This algorithm used for both the pupil and iris

boundaries a component-goodness-of-fit metric for candidate boundary parameters being considered with respect to a given center for the polar coordinate system. The component-goodness-of-fit is defined as

$$C = \sum_{\theta=1}^{n} \left((n-1)||g_{\theta,r}|| - \sum_{\phi=\theta+1}^{n} (||g_{\theta,r} - g_{\phi,r}||) - \frac{I_{\theta,r}}{n} \right) \qquad \text{..... (2.3)}$$

where n is the total number of directions and $I_{\theta,r}$ and $g_{\theta,r}$ are respectively the image intensity and derivatives with respect to the radius in the polar coordinate system. This method is highly accurate with images whose pupil and iris intensities are well separated from the sclera ones and with images that contain no significant noise regions, such as reflections. Otherwise, when dealing with noisy data, the algorithm's accuracy significantly deteriorates [19].

2.2.3 Wildes' Method

An automatic segmentation algorithm based on the circular Hough transform is employed by Wildes [30]. It performed its contour fitting in two steps. First, the image intensity information is converted into a binary edge-map. Second, the edge points vote to instantiate particular contour parameter values. The voting procedure is realized via Hough transforms [49, 50]. The parameter with largest number of votes (edge points) is a reasonable choice to represent the contour of interest. The second step recently called circular Hough transform. There are a number of problems with the Hough transform method. It requires threshold values to be chosen for edge detection and the Hough transform is computationally intensive due to its 'brute-force' approach which may not be suitable for real time applications.

2.2.4 Proença Method

Proença [51] developed an algorithm to segment degraded images acquired in the visible wavelength. The algorithm is divided into two parts: detecting noise-free iris regions and parameterizing the iris shape. The initial phase is further subdivided into two processes: detecting the sclera and detecting the iris. The key insight is that the sclera is the most easily distinguishable region in non-ideal images. Next, he exploited the mandatory

adjacency of the sclera and the iris to detect noise-free iris regions. He stressed that the whole process comprised three tasks that are typically separated in the literature: iris detection, segmentation, and detection of noisy (occluded) regions.

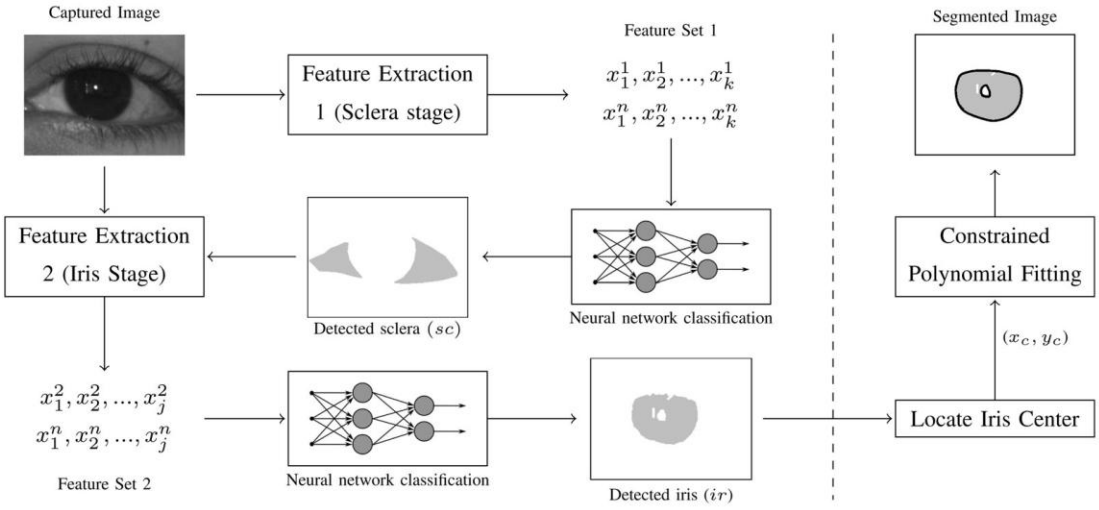

Figure 2.4: Block diagram of Proenca segmentation method [51].

The final part of the method is to parameterize the detected iris region. At last the small classification inaccuracies near iris borders handled using a constrained polynomial fitting method that is both fast and able to adjust shapes with an arbitrary degree of freedom, which naturally compensates for these inaccuracies. Figure 2.4 shows a block diagram of Proenca segmentation method. Proença method is very accurate with noisy images that taken in visible wavelength, but since he depend on sclera on determining the region of iris, the algorithm may fails when the sclera covered with dark colors caused by bad image picked environments or eye diseases.

2.3 Previous Research in Pupil Dilation

As mentioned previously, there are little researches that discussed the problem of pupil dilation and its effect on iris recognition system. In this section we view some of these research.

Daugman's Rubber Sheet Model

Daugman [6] solve the problem of pupil dilation by remaps each point within the iris region to a pair of polar coordinates (r , θ) where r is on the interval $[0,1]$ and θ is angle $[0,2\pi]$. The rubber sheet model takes into account pupil dilation and size inconsistencies in order to produce a normalized representation with constant dimensions. In this way the iris region is modeled as a flexible rubber sheet anchored at the iris boundary with the pupil centre as the reference point. Even though the homogenous rubber sheet model accounts for pupil dilation, imaging distance and non-concentric pupil displacement, it does not compensate for nonlinear dilation of pupil. In the Daugman system, he assumes that when pupil dilates it comprise the iris in linear way but this is not accurate. Many irises is comprised in nonlinear way when their pupil dilates which will affect the performance of iris recognition system.

Hollingsworth, K. Bowyer and P. Flynn analysis

Recently, K. Hollingsworth, K. Bowyer and P. Flynn [52] characterized the effect of pupil dilation on iris recognition performance. they found that when the degree of dilation is similar at enrollment and recognition, comparisons involving highly dilated pupils result in worse recognition performance than comparisons involving constricted pupils. They also found that when the matched images have similarly highly dilated pupils, the mean Hamming distance of the match distribution increases and the mean Hamming distance of the non-match distribution decreases, bringing the distributions closer together from both directions. They further found that when matching enrollment and recognition images of the same person, larger differences in pupil dilation yield higher template dissimilarities, and so a greater chance of a false non-match.

Based on their results, they recommended that a measure of pupil dilation be kept as meta-data for every iris code. Also, the absolute dilation of the two images, and the dilation difference between them, should factor into a confidence measure for an iris match.

Non-linear Normalization Model for Iris Recognition

X. Yuan and P. Shi [53] proposed an iris normalization model for iris recognition, which combines linear and non-linear methods to unwrap the iris region. First, non-linearly transform all iris patterns to a reference annular zone with a predefined λ, which is the ratio of the radii of inner and outer boundaries of the iris. Then linearly unwrap this reference annular zone to a fix-sized rectangle block for subsequence processing. the iris normalization model is illuminated by the 'minimum-wear-and-tear' meshwork of the iris [54] and it is simplified for iris recognition. This model explicitly shows the non-linear property of iris deformation when pupil size changes. And experiments show that it does better than the simplified linear normalization model and will improve the iris recognition performance.

Nonlinear Iris Deformation Correction Based on Gaussian Model

Z. Wei, T. Tan, and Z. Sun [55] introduces a novel algorithm to counteract elastic iris deformation. In their proposed algorithm, for nonlinear iris stretch, the distance of any point in the iris region to the pupil boundary is assumed to be the corresponding distance under linear stretch plus an additive deviation. Gaussian function is employed to model the deviation. In this algorithm, iris images are corrected by compensating the additive deviation between nonlinear and linear iris stretch. Their proposed iris deformation correction algorithm achieves a lower EER, compared to the other two linear and nonlinear normalization methods. This algorithm get good results when the pupil dilation causes non-linear iris deformation, but when the iris deformation is linear, this algorithm will give negative results, or we must know the deformation type of each iris is it linear or not.

2.4 Previous Research in Analyzing Iris Code

Most researchers study causes of texture distortion which distort the texture appearance, but just a few work in analyzing the iris code bits and determining which are the best bits or inconsistent bits. Papers in this topic are very few and there are only six papers until

the writing of this thesis. In this section the previous work in analyzing iris codes is viewed.

K. Hollingsworth, K. Bowyer and P. Flynn Studies on Iris Code

The first published work studied the consistency of the different bits in an iris code is the paper of K. Hollingsworth, K. Bowyer and P. Flynn [56]. Their experiments proved the existence of fragile bits. They found that all subjects had three different regions apparent in their iris codes: areas consistently equal to 0, areas consistently equal to 1, and inconsistent areas. The inconsistent areas tend to occur at the boundaries between regions of zeros and regions of ones. If a bit was equal to one the majority of the time, but was equal to zero 30% of time, then they said that the bit "flipped" in 30% of the iris codes. If a bit was zero the majority of the time, but one for 30% of the time, they still said that the bit "flipped" in 30% of the iris codes. In their study they found that, on average, 15.99% of the bits in an iris code were perfectly consistent; that is, 15.99% of the unmasked bits were always equal to 1 or always equal to 0, for all iris codes for an iris. The subject with the smallest fraction had 4.74% of the bits perfectly consistent, and the subject with the largest fraction had 33.9% of the bits perfectly consistent. Also they found that no gender appears to be difference in the consistency of iris code bits.

S. Ring and K. Bowyer detection method of Iris Texture Distortions

S. Ring and K. Bowyer [57] assumed that some local distortions of the iris texture are not detected at the segmentation stage, and that these generate corresponding regions of local distortion in the iris code derived from the image. So they introduced an approach to detect such regions of local distortion in the iris code through analysis of the iris code matching results. Unlike existing approaches to detecting local distortions in the iris texture focus on analysis of the iris image. In contrast, their approach to detecting local distortions to the iris texture in images of the same iris focuses on analysis of the iris code matching results. This approach has the advantage of making only the most general assumption about the cause of the local distortion in the iris texture. Also, this approach

can be applied independently of and in combination with any improved iris segmentation algorithm. It's the first work that attempts to detect distortions of iris texture through analyzing the iris code matching results.

Minimize the Number of Iris Code Bits Needed for Iris Recognition

G. Dozier, K. Frederiksen, R. Meeks, M. Savvides, K. Bryant, D. Hopes, and T. Munemoto [58, 59] use the concept of fragile bits and demonstrated how the concepts of bit inconsistency and genetic search can be used to minimize the number of iris code bits needed for iris recognition. In addition, they compare two systems: GRIT-I (genetically refined iris templates I) and GRIT-II. their results show that GRIT-I (by evolving the bit mask of iris templates) was able to reduce the number of iris code bits needed by approximately 30% on average. GRIT-II by contrast optimizes the bit mask as well as the iris code bits that have 100% consistency and 100% coverage with respect to the training set. GRIT-II was able to reduce the number of iris code bits needed by approximately 89%.

Chapter 3

Background

In this chapter, basic concepts related to iris recognition and some used techniques in the proposed algorithms are introduced. First, overview of the K-means clustering algorithms is performed. After that the circular Hough transform and Canny edge detection are explained. Finally the morphological operations is described.

3.1 Image K-means Clustering

The K-means algorithm is an iterative technique that is used to partition an image into *k* clusters by assigning each point to the cluster whose center (also called centroid) is nearest. The center is the average of all the points in the cluster that is, its coordinates are the arithmetic mean for each dimension separately over all the points in the cluster.

The basic K-means algorithm we used is:

1. Compute the intensity distribution (also called the histogram) of the intensities.
2. Initialize the centroids with *k* random intensities.
3. Repeat the following steps until the cluster labels of the image does not change anymore.
4. Cluster the points based on distance of their intensities from the centroid intensities.

$$c^{(i)} := \arg\min_j ||x^{(i)} - \mu_j||^2 \qquad \text{..... (3.1)}$$

5. Compute the new centroid for each of the clusters.

$$\mu_i := \frac{\sum_{i=1}^{m} 1\{c_{(i)} = j\} x^{(i)}}{\sum_{i=1}^{m} 1\{c_{(i)} = j\}} \qquad \text{..... (3.2)}$$

Where *i* iterates over all the intensities, *j* iterates over all the centroids and μ_i is the centroids intensities.

Distance is the absolute difference between a pixel and a cluster center. The Distance in our algorithm is typically based on pixel intensity. K-means clustering requires to specify the number of clusters to be partitioned and a distance metric to quantify how close two objects are to each other.

3.2 Circular Hough Transform

The Hough transform [60] is a standard computer vision algorithm that can be used to determine the parameters of simple geometric objects, such as lines and circles, present in an image. It can be described as a transformation of a point in the x, y-plane to the parameter space. The parameter space is defined according to the shape of the object of interest. The circle is actually simple to represent in parameter space, compared to other shapes, since the parameters of the circle can be directly transfer to the parameter space. The equation of a circle is

$$r^2 = (x-a)^2 + (y-b)^2 \qquad \text{..... (3.3)}$$

As it can be seen the circle got three parameters, *r, a* and *b*. Where *a* and *b* are the center of the circle in the *x* and *y* direction respectively and where r is the radius. The parametric representation of the circle is

$$x = a + r\cos(\theta) \qquad \text{..... (3.4)}$$

$$y = b + r\sin(\theta) \qquad \text{..... (3.5)}$$

The parameter space for a circle will belong to R^3 whereas the line only belonged to R^2. As the number of parameters needed to describe the shape increases as well as the dimension of the parameter space *R* increases so do the complexity of the Hough transform. The circular Hough transform can be employed to deduce the radius and centre coordinates of the pupil and iris regions. It works as follow, at each edge point result from previous edge detection step we draw a circle with center in the point with the desired radius. This circle is drawn in the parameter space Figure 3.1 shows this process.

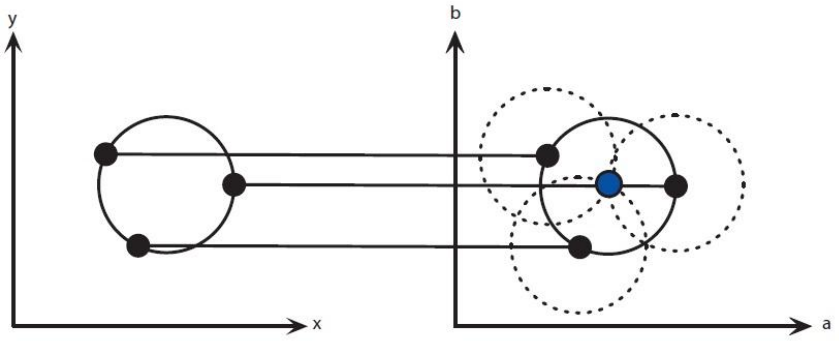

Figure 3.1: A circular Hough transform from the x, y-space (left) to the parameter space (right), this example is for a constant radius.

At the coordinates which belong to the perimeter of the drawn circle we increment the value in our accumulator matrix which essentially has the same size as the parameter space. In this way we sweep over every edge point in the input image drawing circles with the desired radii and incrementing the values in our accumulator. When every edge point and every desired radius is used, we can turn our attention to the accumulator. The accumulator will now contain numbers corresponding to the number of circles passing through the individual coordinates. Thus the highest numbers (selected in an intelligent way, in relation to the radius) correspond to the center of the circles in the image [61].

3.3 Canny Edge Detection

There are many methods for edge detection, but one of the most optimal edge detection methods is Canny edge detection [62]. It receives a grayscale image and outputs a binary map correspondent to the identified edges. It starts by a blur operation followed by the construction of a gradient map for each image pixel. A non-maximal suppression stage sets the value of 0 to all the pixels of the gradient map that have neighbors with higher gradient values. Further, the hysteresis process uses two predefined values to classify some pixels as edge or non-edge. Finally, edges are recursively extended to those pixels that are neighbors of other edges and with gradient amplitude higher than a lower threshold. The Canny edge detection receives the following arguments:

Upper threshold: This parameter is used in the hysteresis operation. Sets the higher values of the gradient map to be considered as edge points.

Lower threshold: This parameter is used in the hysteresis operation pixels with gradient values lower than this are considered as non-edge points.

Sigma of the Gaussian kernel: This parameter defines the standard deviation of the bi-dimensional Gaussian kernel. Higher values increase the power of the blur operator and result in less number of detected edges.

Vertical edges weight: This is used to weight the vertical derivatives in the gradient map construction. It is usually in the [0, 1] interval and is multiplied by the vertical derivative value.

Horizontal edges weight: Similarly to the above parameter, it is the correspondent regarding the horizontal derivatives. It must be noted that, usually, the sum of the vertical and horizontal weight values must be equal to 1.

Scaling factor : This factor used to decrease the image size to decrease the number of edge point.

These arguments are determined according to the applications and environments that use the Canny edge detection. In chapter four we will explain the used values of these arguments in our proposed segmentation algorithm.

3.4 Morphological Operations

The morphological processing refers to certain operations where an object hits a structuring element and is reduced to a more revealing shape. The aim is to transform the signal into a simpler one by removing irrelevant information and can be applied to binary and gray level signals [63] . Most morphological operations can be defined in terms of two basic operations: erosion and dilation. Erosion and dilation are two morphological operations that are very useful in processing binary images. Erosion and dilation, allow groupings of *ones*, represented by white pixels, to be enlarged or shrunk to produce resulting images that either fill grouping gaps or remove small groupings of *ones* as

necessary. Erosion can best be described as a mathematical operator that shrinks groupings of *ones* in binary images. A structuring element, or kernel, represented by a matrix of *ones* and *zeros*, is passed through the original image. During erosion, the resultant image is the set of all structuring element origin locations where the translated structuring element has no overlap with the background of the original image [64]. The eroded image of an image *I* with respect to a structuring element *S*, is the set of all reference points *x* for which *S* is completely contained in *I*:

$$I \ominus S := \bigcup \{x : S + x \subset I\} \qquad \text{..... (3.6)}$$

Ultimately, small groupings of ones and thin lines are removed from the image.

The dilation is the mathematical operator that expands groupings of *ones*, filling 'gaps' or 'holes' in a binary image. The dilation of an image by a structuring element results in an image consisting of all the structuring element origin locations where the reflected and translated structuring element overlaps at least some portion of the image [64]. The dilated image of an object *I* with respect to a structuring element *S*, is the set of all reference points for which *I* and *S* have at least one common point:

$$I \oplus S := \bigcup \{x : S + x \in I\} \qquad \text{..... (3.7)}$$

By repeatedly dilating a binary image, black space (*zeros)* within groupings of *ones* is removed in order to achieve a single homogenous region.

Based on the dilation and erosion operations, the image opening and closing are implemented. Opening corresponds to the image erosion followed by image dilation and the closing corresponds to the opposite (image dilation followed by image erosion). In our iris segmentation algorithm the aim of using Morphological operations is to eliminate eventual noisy data and smooth the information with the purpose of facilitating the segmentation.

Chapter 4

Proposed Algorithms

4.1 Proposed Iris Recognition Algorithms

In this thesis, we propose three techniques to enhance the iris recognition system. As shown in Figure 4.1, the first one is a new segmentation algorithm to handle iris images were captured on less constrained conditions. This algorithm reduces the error percentage while there are types of noise exist, such as iris obstructions and specular reflection. The proposed algorithm starts by determining the expected region of iris using K-means clustering algorithm, then circular Hough transform is used to localize iris boundary, after that some algorithms are proposed to detect and isolate noise regions.

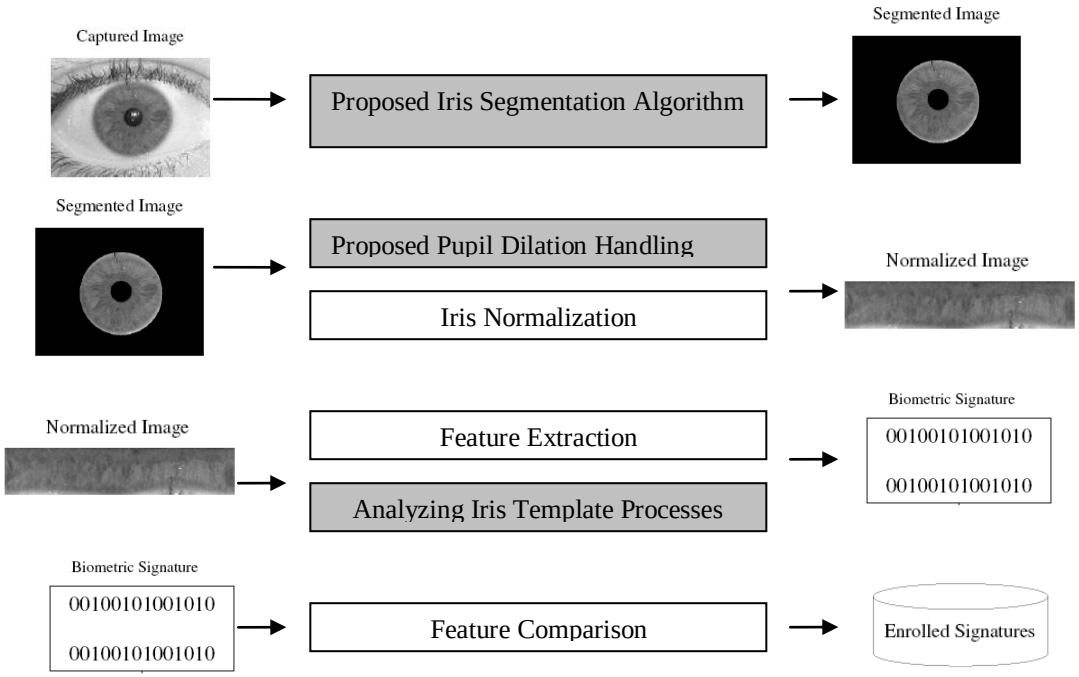

Figure 4.1: Block diagram of proposed enhancing iris recognition algorithms, gray boxes represent our own work.

The second technique study the effect of pupil dilation on iris recognition system, in order to show that the high pupil dilation degrees degrade iris template and affect the performance of recognition system. After that, a limit of dilation degree is determined,

which after it, the iris code will be affected or some of its information will be discarded. This limit can be used to avoid detrimental pupil dilation.

Finally, we analyze the iris code bits to determine the consistent and inconsistent bits, and we compare between the inner and outer regions to find which region contains more inconsistent bits to be excluded from the iris template.

4.2 Proposed Iris Segmentation Method

This section concerns about one of the crucial steps in building an iris recognition system, which is iris segmentation. In this stage, we should accurately extract the iris region despite of the presence of noises such as varying pupil sizes, shadows, specular reflections and highlights. The segmentation stage is important because it is the basis of all further operations, such as normalization and encoding. As mentioned, there are many iris segmentation algorithms were proposed before, and gave an excellent results when iris images picked at Near Infrared camera and in ideal imaging conditions. The accuracy of current segmentation algorithms significantly decreases when dealing with noisy iris images taken in visible wavelength under far from ideal imaging conditions, such as those of the UBIRIS.v1 and v2 database. Our main motivation in this section is to propose a new segmentation algorithm to handle iris images capturing in less constrained conditions.

As mentioned in Chapter two, the segmentation methods can be divided into two categories. The first category applies a certain type of operators like Daugman's Integro-Differential operator, and usually these operators are affected by noises and separability between iris and sclera. The second category uses one type of edge detection filters like Canny or Sobel edge detection followed by circular Hough transform, and these methods are usually very expensive in time.

Our main purpose in this section is to develop a robust iris segmentation method that is not affected by types of noises and at the same time is not expensive in time. As shown in the experiments of Section 5.3, our proposed segmentation algorithm significantly

improves the robustness of the segmentation process even with large noisy iris regions. Figure 4.2 shows the block diagram of our proposed segmentation algorithm.

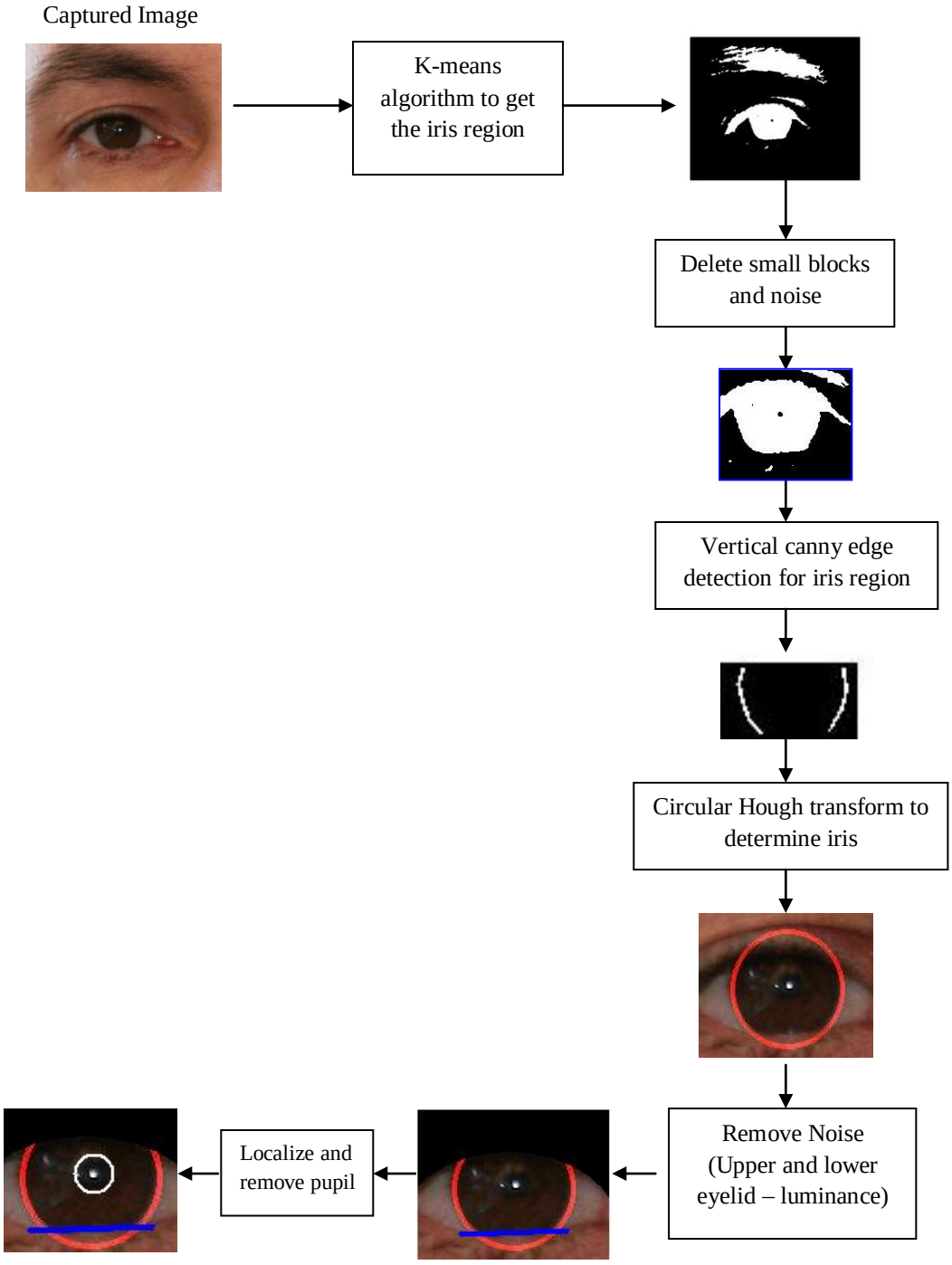

Figure 4.2: Block diagram of proposed iris segmentation method.

Algorithm 4.1 shows the steps of our proposed iris segmentation algorithm.

Algorithm 4.1: Proposed iris segmentation algorithm.

Purpose: Segment noisy irises**.**

Input: Iris image.

Output: Segmented iris without noises

Procedures:

Step 1: Determine the expected region of the iris using K-means algorithm.

a) Separate the red color space from RGB color space of the image.

b) Apply the image clustering algorithm as described in section 3.1 with input number of clusters equals three and the distance is the intensity of pixels.

c) Select the cluster of low intensities (Dark region in the image).

d) Delete small blocks and noise.

Step 2: Apply the edge detection algorithm.

a) Convert RGB color space of the expected iris region to the YCbCr color space, and separate the Y component.

b) Reduce the scaling factor of the image to be 0.5.

c) Apply Canny edge detection.

d) Delete small noise components by applying some morphological operation.

Step 3: Apply circular Hough transform described in section 3.3 on the binary edge image, and select the maximum group of parameter *(a, b, r)* from the accumulator, then find the Cartesian parameters *(x, y, r)* which is the center coordinates and radius of the iris.

Step 4: Upper eyelid localization.

a) Isolate two small rectangles from the outer two sides of iris.

b) Apply horizontal Canny edge detection on these two small rectangles and isolate the noise using morphological operations.

c) Determine the coordinates of upper eyelid on both rectangles.

d) Draw an arc passes the two coordinates of upper eyelid on each rectangle and a radius equals twice the radius of the iris.

Step 5: Lower eyelid localization**.**

a) Take edge map of the lowest half of the iris.

b) Find the best line fit using line Hough transform.

c) If the vote of the line less than certain value, then we assume no lower eyelid occlusion occurs.

Step 5: Isolate specular reflections.

a) Compute the average intensity in the three RGB color spaces for the iris region.

b) If the intensity of each pixel greater than the average intensity computed in the first step plus constant value (explained in more details later), then we consider this pixel as reflection noise pixel.

Step 6: Remove pupil region.

a) Adjust iris image by mapping the values of its bits intensity to new values to focus on dark intensities.

b) Filter the image with median filter.

c) Canny edge detection is used to get the edge map.

d) The circular Hough transform is applied to localize the pupil, assuming that its circular.

The proposed segmentation algorithm avoid starting from the pupil, because the pupil is not always the darkest region in the eye in the noisy images that were taken in a visible wavelength (due to some factors like shadows, specular reflections and highlights). Figure 4.3 shows some noisy eye images, where the pupil is affected by these factors. Also we avoid starting our algorithm from sclera, because some times the sclera is covered by dark colors, and these colors cause errors in determining the region of iris, and as a result the segmentation process will be wrong. Figure 4.4 shows example of unclear sclera that will affect the segmentation results.

Figure 4.3: Noisy iris images selected from UBIRIS v2 iris database. The pupil is affected by specular reflections and highlights in the first and third image. The second image shows a pupil affected by bad luminance and shadows.

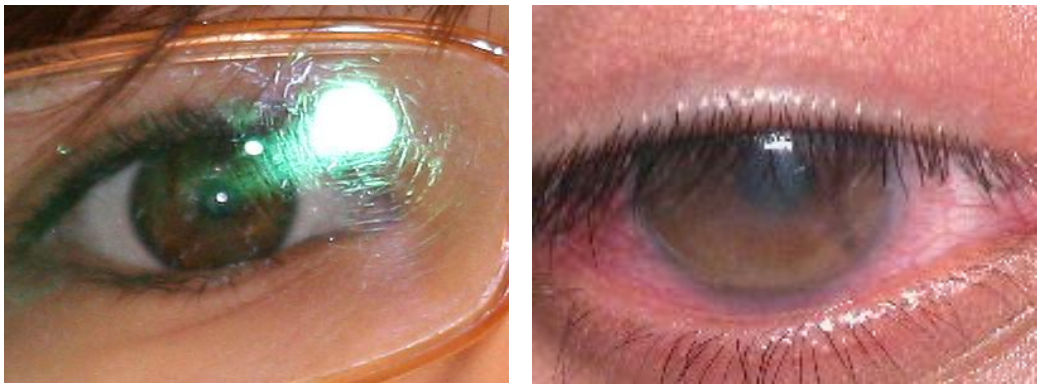

Figure 4.4: Noisy iris images selected from UBIRIS v2 and v1 iris databases respectively. There is a white area more than sclera in the first image and the sclera is covered by dark colors in the second image.

The proposed segmentation algorithm starts by determining the expected region of iris using the K-means clustering algorithm. The output image is used by vertical Canny edge detection to produce edge-maps. The circular Hough transform is applied on the edge image to determine the estimated iris center and radius. We use K-means clustering and vertical edge map to reduce the time of searching for circular Hough transform. Therefore, the circular Hough transform will be applied on the binary edge image which comes from applying the edge detection on masked region, which result from K-means. After determining the iris circle, we apply some new techniques (will be explained in section 4.2.4) to isolate the noisy factors like eyelids, eyelashes, luminance and reflections. At last, we remove the pupil region from the iris region.

4.2.1 Determining Iris Region

One of the most causes of errors in segmentation is the high local contrast (e.g. on eyelashes, eyebrow, glass frame or white areas due to luminance on skin behind eye region) occurs on non-iris regions. Therefore, it is a good idea to avoid such segmentation errors by excluding the non-iris regions in the iris image before the iris localizing step. Obviously, if we can divide the iris image into three regions as iris region, skin region and sclera region, then we can reduce the errors in segmentation and at the same time reduce the searching time at the next steps in segmentation process.

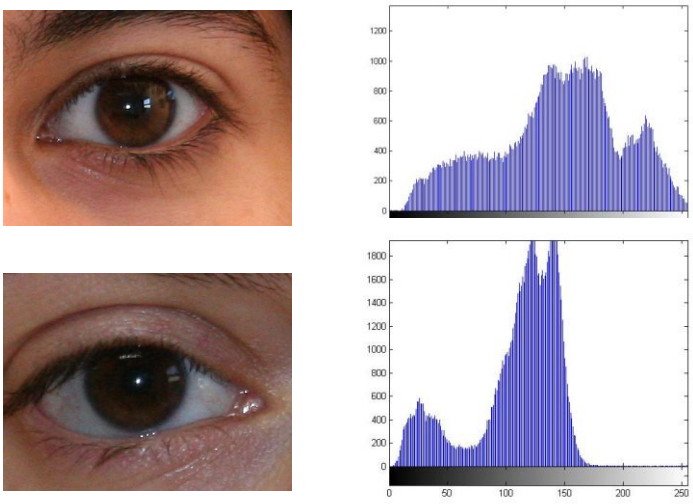

Figure 4.5: The histograms of two eye images from UBIRIS database.

A simple clustering method is proposed to divide the eye image into three different parts based on K-means clustering. The eye image can be divided into three regions. The first region which has small intensity values, consists of the iris (including the pupil) and eyelashes. The second region whish has high intensity values, consists of sclera and some highlights or luminance reflections. The third region is the skin region, its intensity between the previous two regions. Figure 4.5 shows the histogram of two iris images. We can notice from Figure 4.5 the three local maxima, which present the regions of eye images. If we classify the image into four clusters, the region of the iris in images with light irises color (such as blue and green irises) will be reduced and the segmentation process will fail. This is because the iris boundary may lie outside the region of iris. While if we divide the image into two clusters, the region of iris will become wider, usually more than the half of the image area. This will insert non-iris regions to the iris region which will cause errors and increase the execution time of Hough transform in the next step. The K-means clustering algorithm is effective, because it concerns about the darkest region only, and we will not worry about other two clusters. As mentioned in the background Chapter, the K-means algorithm is an iterative technique that used to partition an image into *K* clusters by assigning each point to the cluster whose center (also called centroid) is the nearest. The center is the average of all the points in the cluster, that is, its coordinates are the arithmetic mean for each dimension separately over all the points in the cluster. The distance is the absolute difference between a pixel

and a cluster center. The Distance in our algorithm is typically based on pixel intensity. K-means clustering requires that to specify the number of clusters to be partitioned, it is found experimentally that when K equals three, the algorithm gives the best results.

First, we separate the red color space from the RGB color space of the image, because it contains the most of the iris details. Then, we apply the image K-means clustering algorithm as described in Chapter three on the red color space of the image. After clustering, the resulted image is handled with some morphological operations (as described in Section 3.4) to delete small blocks and noise. We choose the nearest block from the center to discard the eyebrow region. Figure 4.6 shows the result when we apply the clustering algorithm on some images. White regions present the darkest region (which is the region of iris and eyelashes) in the image. The black regions present region of sclera and some highlights or luminance reflections. The gray regions is the region of skin which its intensity between the previous two regions. As we can see in Figure 4.6, the white area covers the iris, eyelashes and some times eyebrow, but excludes luminance and specular reflections. This is very helpful in reducing the handled areas. The clustering algorithm reduces the region of iris by more than 70%. Consequently, the searching time of the next steps also will be reduced.

(a)

(b)

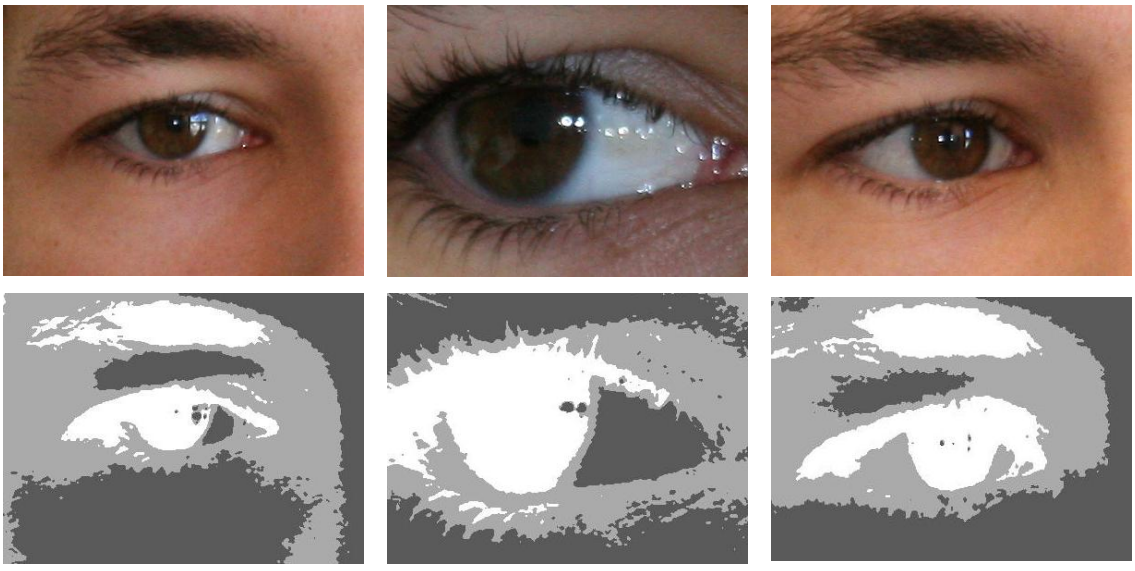

Figure 4.6: Illustration of the results of K-mean clustering on some images (a) real images. (b) Clustering result images, white regions represent the estimated iris region.

4.2.2 Edge Detection

To find the edge points in the iris image, Canny edge detection is used as described in Section 3.3. The implemented Canny edge detection has six arguments. We adjust the upper threshold and the lower threshold inputs experimentally to make the algorithm suitable for the noisy iris images. In our algorithm, to extract the iris-sclera border, we select high value for vertical edges weight and low value for horizontal edges weight, because we interested only on vertical edges. These values adjusted only once for the whole database (to be suitable for environment conditions) and do not need to be computed for each iris image. This process decreases the errors result from the horizontal edges due to eyelashes and eyelids. The scaling factor equals 0.5 to reduce the size of the image to the half. This scaling reduction will reduce the searched pixels to the half. We found that if we reduce the scaling factor to value less than 0.5, many edge points will disappear and this will cause errors in localizing the iris boundary.

In our algorithm, we did not use the grayscale image as input. Instead, we experimentally find that the best image used is the Y component of YCbCr color space. We first convert the image from RGB to YCbCr color space, and then the Y component is separated. Finally, Median filter is applied to the Y component image to handle small noises and to smooth the image. Remember that the edge detection applied only on the reduced area result from the clustering step. Figure 4.7 shows the results of applying the Canny edge detection on sample images. Figure 4.7(b) shows the Y component of YCbCr color space, we notice that this component reduces the effect of luminance, specular reflection and the red regions in the sclera. As a result, more edge points will be avoided to be processed in **C**ircular **H**ough **T**ransform (CHT) step. Figure 4.7(c) shows images after applying Canny edge detection, we see that the biggest two connected components are the iris' boundaries, but numbers of small noise components is still exist. We can reduce the number of small noise components by applying some morphological operations. The result is shown in Figure 4.7(d). Although some noise components are still exist, we reduce the edge points that will be processed or searched by CHT in a very good way. Note that the binary edge images in Figure 4.7(c) and (d) is viewed after scaling by factor of 0.5. Also to reduce edge points that will be searched by CHT as much as possible.

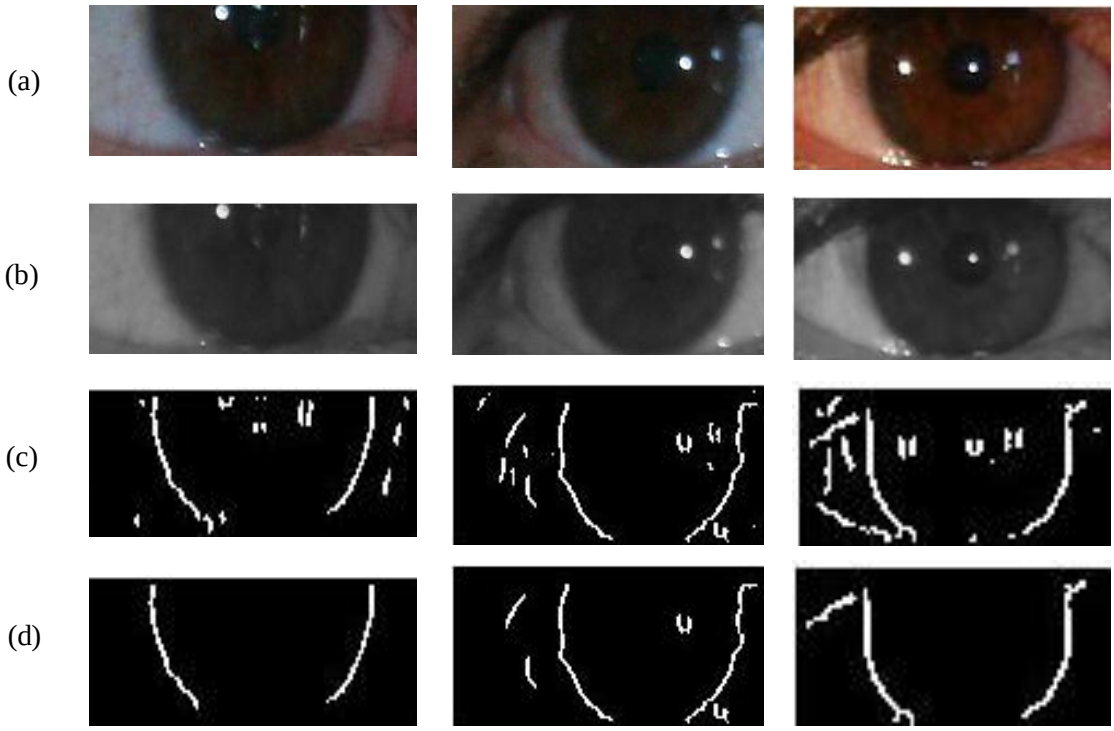

Figure 4.7: Illustration of the results of applying the Canny edge detection on some images (a) real images result from clustering step. (b) Y component of the image after convert it to YCbCr color space. (c) Binary image results from Canny edge detection using scaling factor equals 0.5 (d) Binary image after removing small blocks and noises.

4.2.3 Circular Hough Transform

As mentioned in Chapter three, the circular Hough transform belong to R^3 space, so the complexity of the Hough transform is $O(n^3)$. Therefore, to reduce the time of its execution, we use the three methods which explained in previous steps :

1. Scaling factor: which reduces the image size and causes reduction in the edge points.
2. K-means clustering: to reduce the searching area, and to reduce the edge points when Canny edge detection is applied.
3. The usage of morphological operations: to remove small blocks and noise in the binary edge image.

After applying the circular Hough transform described in Section 3.3 on the binary edge image, we select the maximum group of parameters *(a, b, r)* from the accumulator, and

then find the Cartesian parameters *(x, y, r)* to determine the iris' on the image. Figure 4.8 shows some examples. As shown in this figure, the iris' location boundary is detected and white circles fit irises precisely, despite the presence of some noise factors, like specular reflections, iris' occlusion by eyelids and eyelashes. Also, we notice that irises are localized correctly regardless of their size, This is another benefit of our segmentation algorithm.

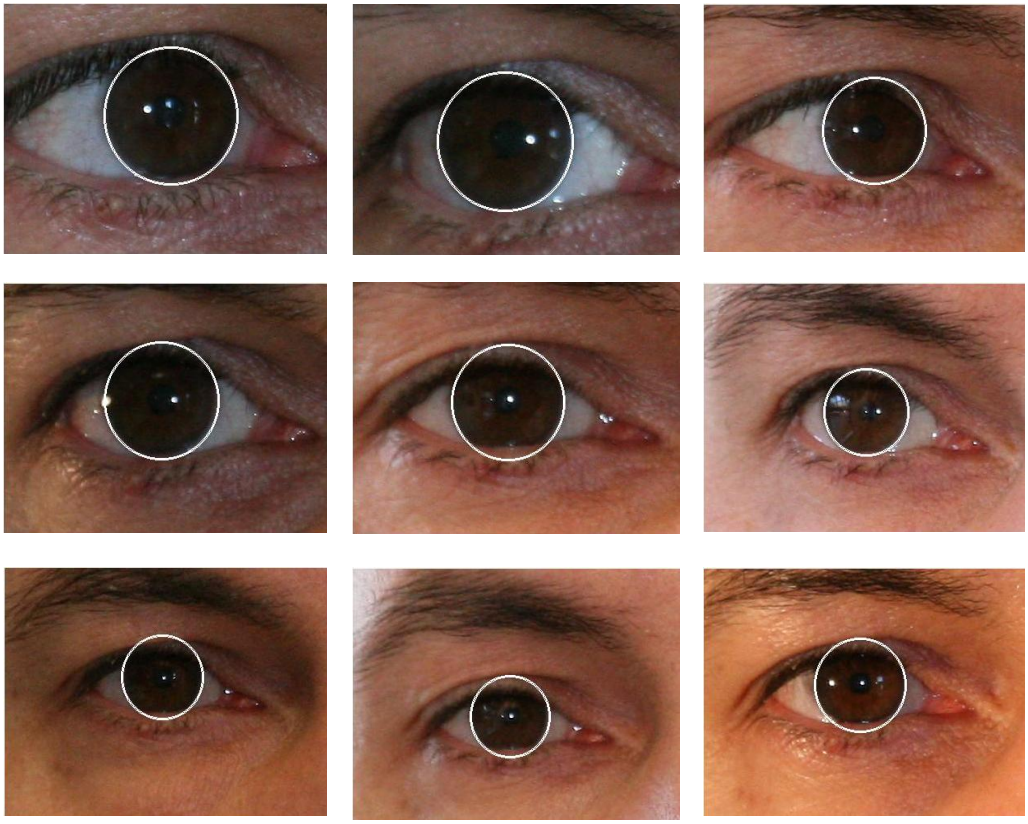

Figure 4.8: Samples of segmented irises from UBIRIS v2.

4.2.4 Isolating Noise

In non-cooperative iris recognition, the user has little or even no active participation in the image capturing process [65]. As a result, the iris' images are often captured with more noisy artifacts, such as reflections, occlusions by eyelids or eyelashes, shadows, etc. It has been reported that the most localizations fails occur on non-iris regions due to the high local contrast. Therefore, to avoid such localizations fails, we must exclude the non-

iris regions and handle all sources of errors. In this subsection, we will explain how the proposed segmentation method handle each of them.

Upper Eyelid Localization

Researchers use many methods to localize the eyelid of the iris (e.g. edge detection, Integro-differential operator and line Hough transform), which captured in the ideal environments. Therefore, these methods are not effective to be used in noisy iris images, because the intensity contrast of iris and eyelid can be very low, especially for heavily pigmented (dark) irises, such as in Figure 4.3. We propose a new method to localize the eyelids by detecting it in the sclera region. We detect the eyelids in the sclera, because the intensity contrast of the sclera and the upper eyelid is very higher than the intensity contrast of the iris and the upper eyelid. The following steps explain the upper eyelid localization algorithm.

a) Isolate two small rectangles from the outer two sides of the iris. Each one starts vertically from the center of the iris and extends to value more than the iris center as shown in Figure 4.9.

b) Apply any type of horizontal edge detection on the two rectangles (e.g. Canny edge detection) and isolate the noise using morphological operations.

c) Determine the coordinates of upper eyelid on both rectangles. Assuming that it is the biggest horizontal edge line on each rectangle.

d) Draw an arc that passes through the two coordinates of the upper eyelid on each rectangle and a radius equals the double of the radius of the iris. The center of the arc is computed using the following steps.

Let the coordinates of the upper eyelid on the first rectangle be (x_1 , y_1), and coordinates of the upper eyelid on the second rectangle be (x_2 , y_2). The line passing through the two coordinates of the upper eyelid on each rectangle is given by the equation :

$$ax + by + c_{\text{hori}} = 0 \quad \text{..... (4.1)}$$

where $a = y_2 - y_1$, $b = x_1 - x_2$, $c_{\text{hori}} = x_2y_1 - x_1y_2$

Let (p, q) be the midpoint of the horizontal line joining (x_1 , y_1) and (x_2 , y_2). Then The equation of the perpendicular to the horizontal line at midpoint of the two points (x_1 , y_1) and (x_2 , y_2) is :

$$bx - ay + c_{vert} = 0 \quad \ldots\ldots\ldots (4.2)$$

where $c_{vert} = aq - bp$

Then, we find the point that lies on the vertical line and at a distance of the double of the iris' radius from the middle of the horizontal line as shown in Figure 4.9.

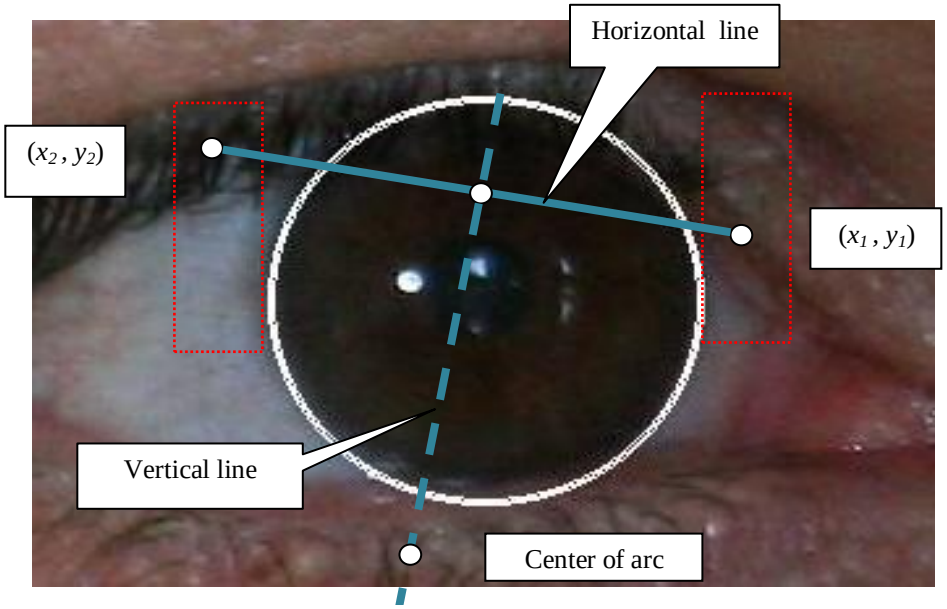

Figure 4.9: Upper eyelid localization model.

Figure 4.10 shows sample images of UBIRIS v2 and v1, after using our method to localize the upper eyelid of the iris. Note that, due to the use of arc in the proposed method, the iris' region will not lose non-noise regions such as happened when using Line Hough transform. We can see from Figure 4.10 that our algorithm isolates the upper eyelid accurately, even if the intensity contrast of the iris and the eyelid are very low, and could not be isolated using normal processes like line Hough transform or Integro-Differential operator of Daugman. The effectiveness of our algorithm is due to the usage of the intensity contrast between the sclera and the upper eyelid rather than the iris and the upper eyelid. Also, we can see that this algorithm still working, when a huge area of iris is occluded by upper eyelid.

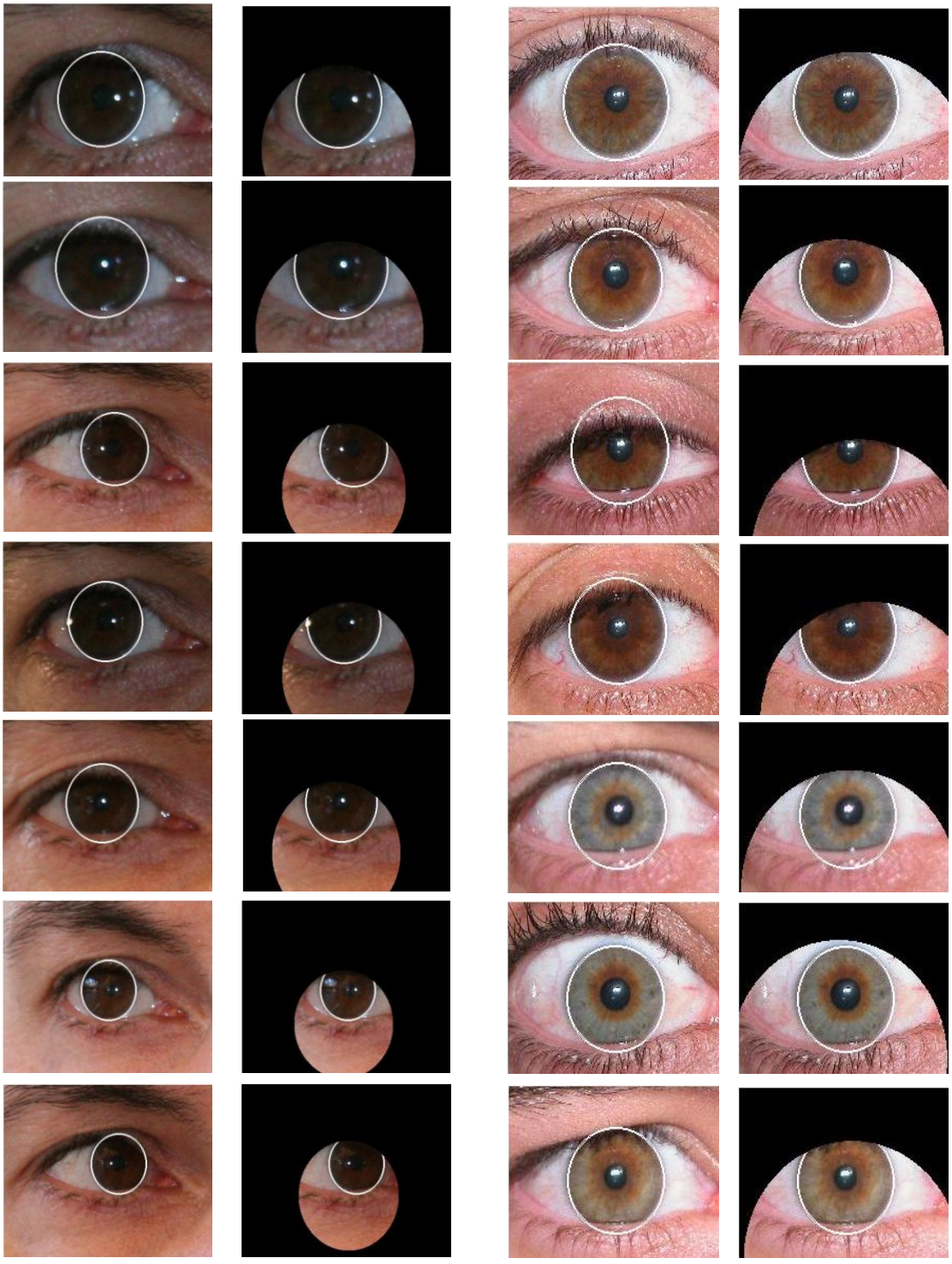

(a) (b) (c) (d)

Figure 4.10: Upper eyelid localization algorithm (a) segmented images from UBIRIS v2. (b) segmented images from UBIRIS v2 after using the proposed upper eyelid localization. (c) segmented images from UBIRIS v1. (d) segmented images from UBIRIS v1 after using the proposed upper eyelid localization.

Lower Eyelid Localization

To localize the lower eyelid of the iris, we use the Line Hough transform, because most of the occlusions of the lower eyelid is approximately linear. We first, apply the Canny edge detection to the lowest half of the iris, and then the best line fit using Line Hough transform is found. If the vote of the line is less than a certain value, then we assume no lower eyelid occlusions occur.

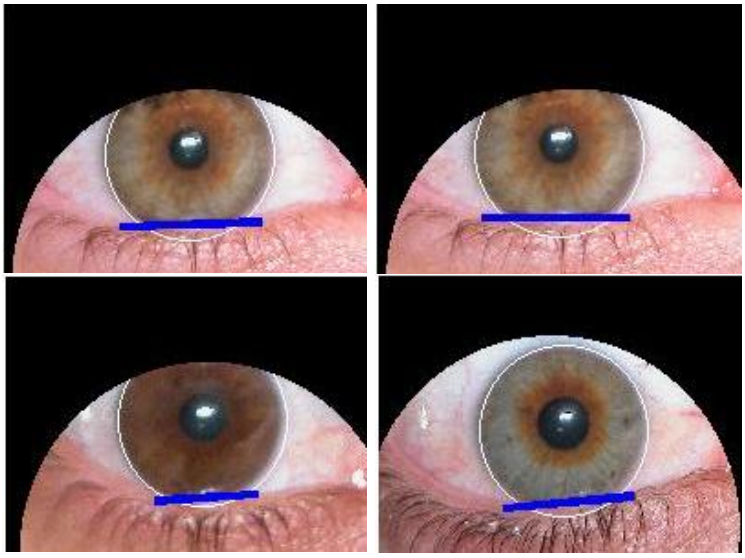

Figure 4.11: Lower eyelid localization samples using UBIRIS v1 database.

Figure 4.11 shows some examples after localizing the lower eyelid. The blue line represents the largest edge line that separates the iris and the lower eyelid. We notice that the lower eyelid isolation process is easier than the upper eyelid, because there is no eyelashes occlusion, and usually the occluded area of the iris due to the lower eyelid is less than the occluded area of the iris due to the upper eyelid.

Isolating Specular Reflections

Specular reflections can be a serious problem, when there are noisy images processed by the iris recognition system. We propose a new simple reflection removal method in two steps :-

1. Compute the average intensity of the iris region in the three RGB color spaces (After upper and lower eyelids removal).
2. Test the intensity of each pixel in the iris, and if the intensity of the pixel in certain color space is greater than the average intensity computed in the first step plus constant value, then consider this pixel as a reflection noise pixel. The constant value is adjusted only once for the whole images.

(a)

(b)

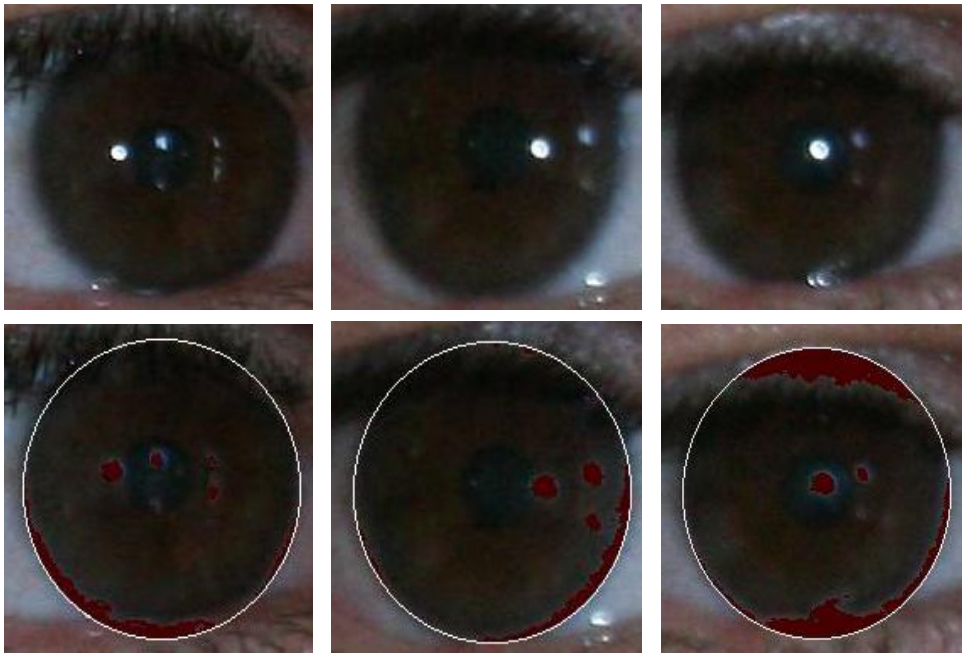

Figure 4.12: Isolating reflections from irises in the proposed algorithm (a) image with reflections. (b) detect the reflection regions (marked with red color).

Figure 4.12 views some images after localizing the specular reflections. The pixels which are distinctive with a red color are masked to be isolated, when iris template code is extracted. We notice that specular reflection and highlight regions are determined precisely, even if there is a light or occluded small regions as shown in Figure 4.12. Note that this process can also discards some redundant white spaces, that might be resulted from off-angle picked images.

4.2.5 Removing Pupil Region

Pupil removal is left to be performed in the last step, because one of the major differences between the eye's images in the noisy databases were captured under visible wavelengths,

and with those images taken under **N**ear **I**nfra**R**ed (NIR) illumination is that the intensity contrast of the iris and the pupil are be very low, especially for heavily pigmented (dark) irises, such as in Figure 4.6 and 4.9. If we try to localize the pupil directly, we will fail. Therefore, the best method is to enhance the image iris to make the pupil appearing using the contrast enhancement method [24]. The following steps explains the pupil removal process.

a) Adjust iris' image by mapping the intensity values of its bits to new values to focus on dark intensities. This step makes the difference between the iris and the pupil more clear.

b) Apply median filter to reduce the noise factors and to preserve the edges.

c) Canny edge detection is used to get the edge map.

d) The circular Hough transform is applied to localize the pupil, assuming that it is circular. The pupil radius is set to be from 1/10 of the iris' radius as the lower limit, to 7/10 of the iris' radius as the upper limit.

Figure 4.13 shows the steps of this algorithm using an image from UBIRIS v2. Note that, all previous steps are applied only on the inner square of the iris to reduce the time execution and to avoid errors that may happened due to the edge points outside the pupil region. As we can see in Figure 4.13, the pupil localization successes even if the intensity contrast of the iris and the pupil are very low.

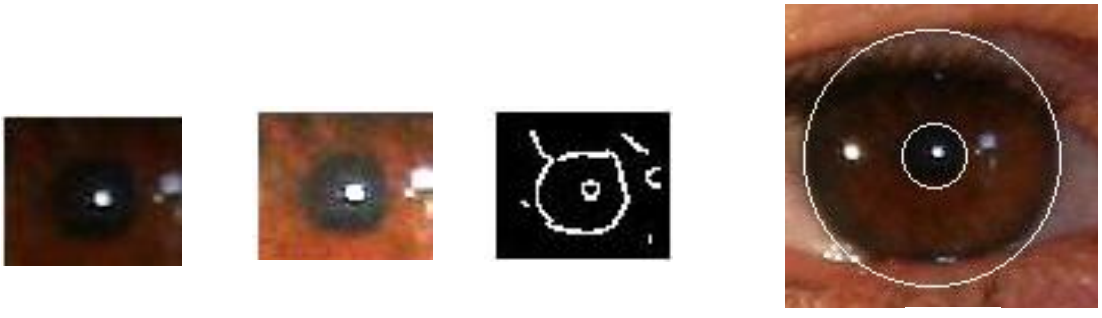

(a) (b) (c) (d)

Figure 4.13: Steps of Pupil removal algorithm (a) the inner square of the iris. (b) result of adjust image in (a). (c) result of Canny edge detection. (d) result of the circular Hough transform.

4.3 Pupil Dilation

Iris recognition systems are facing many problems such as eyelids, eyelashes, specular reflections and pupil dilation. Researchers are interested a lot in the problems that cover parts of the iris region or make some noise on it. But, few researches try to discuss the problem of pupil dilation, because the effect of this problem is relatively not apparent to the eye. In Daugman's early work the normalization of the iris makes it possible to compare two images of different sizes. However, information about the degree of pupil dilation is discarded. In this section, we show that the pupil dilation degrades iris template and affect the performance of recognition system. To show this, the following steps are followed.

Algorithm 4.2: Analyzing the effect of pupil dilation algorithm.

Purpose: Analyzing the effect of pupil dilation**.**

Input: Iris images.

Output: Proof that the pupil dilation reduces the performance of the iris recognition systems.

Procedures:

Step 1: Gather dataset of iris' images that contains many irises for the same class which have widely variations in pupil dilation degrees.

Step 2: Segment irises in the selected dataset and encode each iris in it to produce its iris code.

Step 3: Compare each iris' template in the dataset with all other iris' templates in the dataset.

a) compare irises in the same class to generate intra-class comparisons distribution.

b) compare irises in different classes to generate inter-class comparisons distribution.

Step 4: Calculate the FMR and FNMR for this dataset.

Step 5: Exclude irises which have a dilation degree more than 0.5 from the dataset and repeat steps from 1 to 4.

Step 6: Compare the results.

As shown in Algorithm 4.2, we compare the error rates for two datasets, the first dataset contains all the degrees of pupil dilation. The second dataset contains only irises of small pupil dilation degrees. If the pupil dilation affects the performance, the error rate of the second dataset must be less than the first dataset error rate. In section 5.2, experimental results show that the pupil dilation affects the performance of the iris recognition systems.

Algorithm 4.3: Determining the pupil dilation limit algorithm.

Purpose: Determining the pupil dilation limit**.**

Input: Iris images.

Output: Pupil dilation limit.

Procedures:

Step 1: Gather dataset of iris images that contains many irises for the same class, which have widely variations in pupil dilation degrees.

Step 2: Segment irises in the selected dataset and encode each iris in it to produce its iris' code.

Step 3: Compare each iris template in the dataset with all other iris templates in the dataset.

(a) compare irises in the same class to generate intra-class comparisons distribution.

(b) compare irises in different classes to generate inter-class comparisons distribution.

Step 4: Calculate the FMR and FNMR for this dataset.

Step 5: Exclude irises which have a dilation degree more than a certain limit X from the dataset, where the first value of X equals the highest pupil dilation degree in the dataset.

Step 6: Decrease the value of X gradually and repeat the steps from 1 to 5.

Step 7: Get the limit value X that minimizes the error rates.

Many previous researches try to test the effect of pupil dilation on iris' template and show how do the different degrees of dilation affect the performance of an iris biometrics system. But no prior work has quantified what is the degree of pupil dilation that is if the dilation exceeds it, the performance of an iris biometrics system will be affected. In other

words the pupil dilation limit that the pupil dilation in the iris should not exceeds it will be determined to get the best results. To find this limit the following steps in Algorithm 4.3 are proposed. Experimental results in section 5.2 show that there is a pupil dilation limit that when dilation degree exceeds it, the performance of the iris recognition system will be affected.

4.4 Analyzing Iris Code Bits

Identification and verification of humans using iris biometrics are affected by many factors. Contact lens artifacts, occlusion by hair, pupil dilation, eyelids, eyelashes, and specular highlights distort texture appearance and cause the FMR and FNMR errors to increase. Recently, a new problem is found that also affect the performance of iris recognition system, it's the inconsistent bits or fragile bits. For a given iris, a bit in its iris code will be called as "fragile" or inconsistent, if there is any substantial probability of it to be ending up with a zero for some images of the iris, and a one for other images of the iris. These bits can significantly degrades iris recognition performance. Therefore the existence of inconsistent bits in the dataset will be investigated using the following steps in Algorithm 4.4.

Algorithm 4.4: Analyzing the iris code algorithm.

Purpose: Analyzing the iris code**.**

Input: Iris images.

Output: Proof that the iris code contains some inconsistent bits.

Procedures:

Step 1: Gather dataset of iris images have that high detailed texture.

Step 2: Segment irises in the selected dataset and encode each iris in it to produce its iris code.

Step 3: Compare the templates of irises for the same person to determine which bits is consistent or inconsistent. Let X be the percent of bit retention (if X = 70% means that this bit remains zero or one in 70% of iris images for the same person).

- If any bit keep its value for a percent more than X, it is labeled as consistent.
- If any bit keep its value for a percent less than X, it is labeled as inconsistent.

The value of X can be selected to be suitable for the capturing device and the selected dataset. More discussion and explanation for these steps and results will be viewed in section 5.5.

After determining the consistent and inconsistent bits in our dataset, we can use the result in several ways. Here, we use the consistent and inconsistent bits to study the regions where these bits exists in. Algorithm 4.5 explains the steps of our method to determine which regions are significant more than the others in the iris code. Section 5.5 describes in details the results of this algorithm.

Algorithm 4.5: Determining the best regions in iris code algorithm.

Purpose: Determining the best regions in the iris code**.**

Input: Iris images.

Output: Proof that the inner regions in iris code are better than the outer regions in iris code.

Procedures:

Step 1: Gather dataset of iris images which have high detailed texture.

Step 2: Segment irises in the selected dataset and encode each iris in it to produce its iris code.

Step 3: Divide the iris code to four parts, each part with 5x480 bits

Step 4: Mask each part separately and execute matching test the same as performed in Algorithm 4.2 and compute the FNMR for each one.

Step 5: Compare the results

Chapter 5

Results and Discussion

In this chapter, we describe the common public and freely available iris image databases, which will be used in this thesis. Then, the selected and used datasets in the experiments will be viewed. Finally, we will show and discuss the results of our experiments.

5.1 Public Iris Databases

The fair comparison between recognition methods needs similar input data to compare and evaluate their results. Therefore, standard iris' databases assume high relevance, and become indispensable in the development process. There are many iris' image databases available freely on the Internet such as CASIA, UBIRIS, MMU [66], ICE [67], WVU [19] and UPOL [68]. In this section, we describe the main characteristics of the common public and freely available iris images databases for biometrics purposes, which will be used in the experiments.

5.1.1 CASIA Database

CASIA Iris Image Database (CASIA-Iris) developed by Chinese Academy of Sciences Institute of Automation research group [69]. This database has been released to the international biometrics community and updated from CASIA-IrisV1 to CASIA-IrisV4 since 2002. More than 3,000 users from 70 countries or regions have downloaded CASIA-Iris and much excellent work on iris recognition has been done based on these iris image databases.

CASIA-IrisV1

CASIA Iris Image Database Version 1.0 (or CASIA Iris-V1) is probably the first iris image database publicly available to iris recognition researchers and has been widely used. It includes 756 iris images from 108 eyes, hence 108 classes. For each eye, 7 images are captured in two sessions, where three samples are collected in the first and four in the second session. Its images were captured within a highly constrained capturing environment, which conditioned the characteristics of the resultant images. They present

very close and homogeneous characteristics, and their noise factors are exclusively related with iris obstructions by eyelids and eyelashes.

CASIA-IrisV2

CASIA Iris Image Database Version 2.0 (CASIA-IrisV2) includes two subsets captured with two different devices: Irispass-h developed by OKI and self-developed device CASIA-IrisCamV2. Each subset includes 1200 images from 60 classes.

CASIA-IrisV3

CASIA-IrisV3 includes three subsets which are labeled as CASIA-IrisV3-Interval, CASIA-IrisV3-Lamp, CASIA-IrisV3-Twins. CASIA-IrisV3 contains a total of 22,035 iris images from more than 700 subjects. All iris images are 8 bit gray-level JPEG files, collected under near infrared illumination. Almost all subjects are Chinese except a few in CASIA-IrisV3-Interval. Because the three data sets were collected in different times, only CASIA-IrisV3-Interval and CASIA-IrisV3-Lamp have a small overlap in subjects. This database is used by many researchers to investigate the performance of their algorithms. CASIA-IrisV3 includes three subsets which are labeled as

1. CASIA-IrisV3-Interval : Iris images were captured very good image quality with extremely clear iris texture details.
2. CASIA-IrisV3-Lamp : Iris images have nonlinear deformation due to variations of visible illumination. A lamp was turned on/off close to the subject to introduce more intra-class variations when this database is collected. As a result of turning a lamp on/off close to the subject the pupil will dilate and shrink and irises with different pupil dilation degree will be generated. CASIA-IrisV3-Lamp contains 16213 iris images for 819 classes
3. CASIA-IrisV3-Twins : The first publicly available twins' iris image dataset.

CASIA-IrisV4

CASIA-IrisV4 is an extension of CASIA-IrisV3 and contains six subsets. The three subsets from CASIA-IrisV3 are CASIA-Iris-Interval, CASIA-Iris-Lamp, and CASIA-Iris-Twins respectively. The three new subsets are CASIA-Iris-Distance, CASIA-Iris-

Thousand, and CASIA-Iris-Syn. CASIA-IrisV4 contains a total of 54,601 iris images from more than 1,800 genuine subjects and 1,000 virtual subjects. All iris images are 8 bit gray-level JPEG files, collected under near infrared illumination or synthesized. The six data sets were collected or synthesized at different times and CASIA-Iris-Interval, CASIA-Iris-Lamp, CASIA-Iris-Distance, CASIA-Iris-Thousand may have a small inter-subset overlap in subjects.

CASIA-Iris-Interval is selected to be used in our analyzing iris code experiment, because the iris images are captured very clear. CASIA-Iris-Interval is well-suited for studying the detailed texture features of iris images.

5.1.2 UBIRIS Database

The main focus of the UBIRIS database [70] is to minimize the requirement of user cooperation, i.e., the analysis and proposal of methods for the automatic recognition of individuals, using images of their iris captured at-a-distance and minimizing the required degree of cooperation from the users, probably even in the covert mode. The UBIRIS database has two distinct versions:

UBIRIS.v1 - This version of the database is composed of 1877 images collected from 241 eyes during September, 2004 in two distinct sessions. It simulates less constrained imaging conditions. The images in this database were saved as TIFF format in RGB color representation. Nikon E5700 camera was used to capture this database and it's the first iris database captured in visible wavelength. It is public and free available.

UBIRIS.v2 - The second version of the UBIRIS database has over 11,000 images (and continuously growing) and more realistic noise factors. Images were actually captured at-a-distance and on-the-move.

5.2 Hardware and Software Environments

To evaluate the proposed algorithms, we implement our algorithms described in Chapter four using MATLAB 7.0 software. The environment where the experiments are performed in is Compaq PC, Core 2 Due Intel Pentium Processor (2.00 GHz), with 1GB

RAM and Windows 7 operating system. In our experiments, we use three free public iris' databases (UBIRIS v1, CASIA v3 and CASIA v4). We use the whole images of UBIRIS v1 in the first experiment, but we select some images from CASIA v3 and CASIA v4 databases to concentrate on certain types of errors in the second and third experiments. In order to evaluate our algorithms in the whole iris recognition system, some functions from Masek's iris recognition algorithms are used in the stages of normalization and parts of feature extraction.

5.3 Results of Proposed Segmentation Algorithm

In the proposed segmentation algorithm, we start the implementation with K-means clustering followed by edge detection and circular Hough transform as shown in Figure 4.1. We assume that both the iris and the pupil have circular form. So, every circle is completely described by the values of its center (x , y) and its radius r. We consider the segmentation is accurate when the two circles of the iris and the pupil fall exactly into the iris and the pupil borders.

After applying the proposed iris segmentation algorithm on UBIRIS v1 (Session 1), we get the segmented images as shown in Figure 5.1. After that, we compute the accuracy (the segmentation is accurate when the two circle of iris and pupil fall exactly into the iris and pupil borders) of the resulted images.

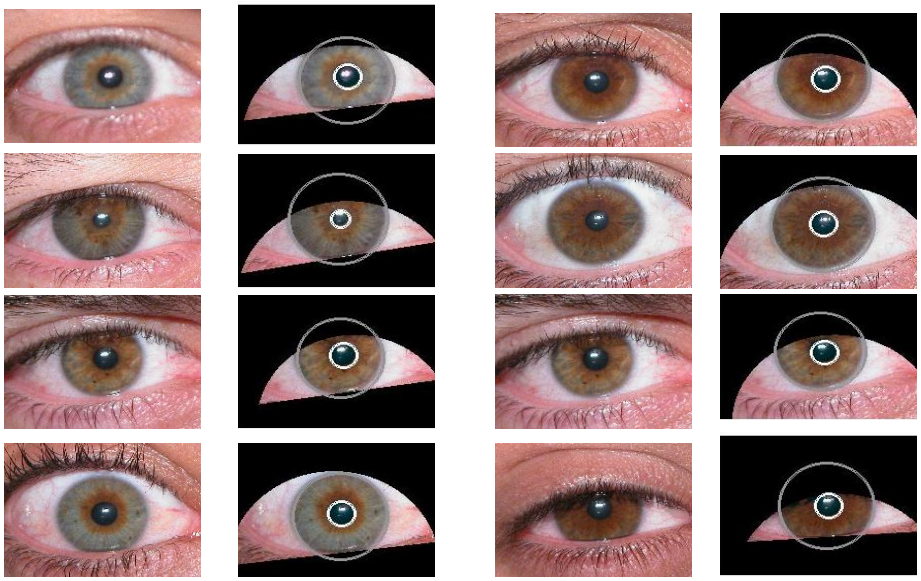

Figure 5.1: Examples of correct segmented irises.

Table 5.1 compares the accuracy of the previous segmentation algorithms (the experiments executed approximately in the same hardware environments) described in Sections 2.1 as viewed in [19] and the proposed algorithm.

Table 5.1: Comparison between the accuracy of proposed algorithm with some previous algorithms.

Method	Accuracy	Time (s)
Daugman	95.22%	2.73
Camus and Wildes	98.68%	1.95
Martin-Roche	77.18%	2.91
Proposed	98.76%	1.49

As the results shown, the proposed algorithm accuracy is better than Daugman and Wildes algorithms. At the same time the execution time of our segmentation algorithm is the lowest one, because the different proposed steps that applied to reduce the searching areas in circular Hough transform. The proposed algorithm failed in segmenting noisy irises when eyelids and eyelashes obstruct big portions of the iris (more than 60%) or when the upper or the lower eyelids cover the pupil of the iris (Note that the most of segmentation methods fail in theses cases). Figure 5.2 gives examples of failed iris segmentation images.

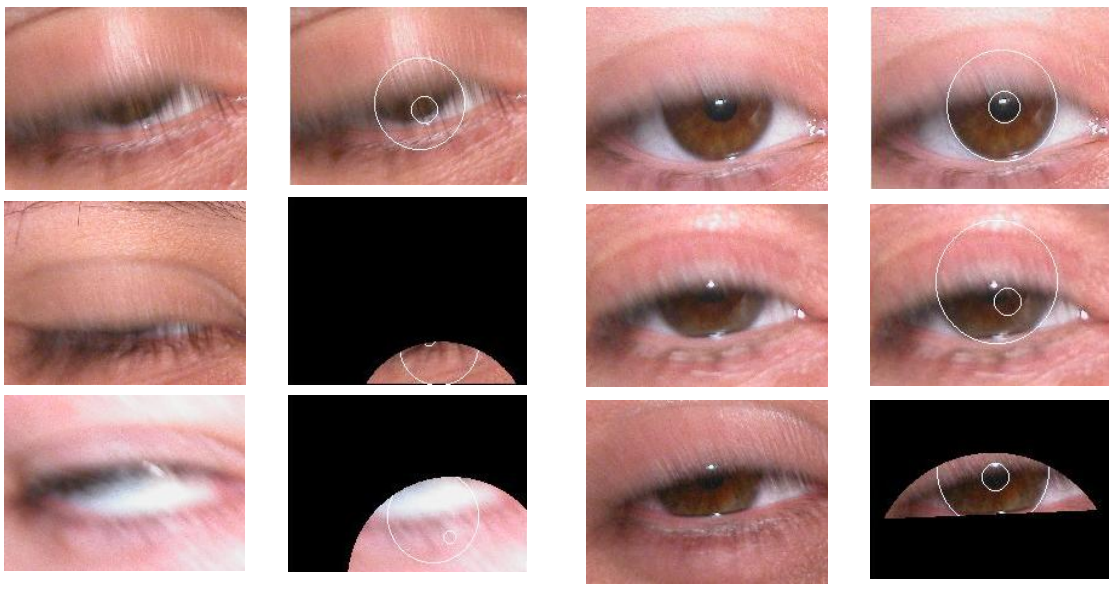

Figure 5.2: Examples of failed segmented noisy irises when eyelids and eyelashes obstruct a big portions of the iris.

In the second column of Figure 5.2, our segmentation algorithm failed, because the iris is approximately covered completely by eyelids. In the fourth column, our segmentation algorithm success in localizing the iris boundary, but it fails in localizing the pupil boundary when it is covered by eyelids, and also fails in isolating the eyelids regions when the iris image is blurred due to fast movements while capturing the image.

To evaluate the performance of the proposed segmentation method in the whole recognition system, we implement the other three stages (normalization, encoding, comparisons). Some functions from Masek's iris recognition algorithm are used [71]. The implemented system is used to generate the iris' template code for every iris. To draw the match and non-match distributions for this database, each iris image in the database is compared with the other all irises in the database. For the UBIRIS v1 Iris Database session1, the total number of comparisons equals 1,448,410 where the total number of intra-class comparisons equals 2410 and that of inter-class comparisons equals 1,446,000.

During the comparison stage, the HD is used as the metric of dissimilarity between two considered iris' codes *codeA* and *codeB*:

$$\mathrm{HD} = \frac{\|(codeA \bigotimes codeB) \bigcap maskA \bigcap maskB\|}{\|maskA \bigcap maskB\|}, \quad \text{.....(5.1)}$$

where *maskA* and *maskB* are the masks of *codeA* and *codeB*, respectively. A mask as proposed by Daugman [72] signifies whether any iris region is occluded by eyelids, eyelashes, luminance, so it reflects the achieved results. HD is therefore a fractional measure of dissimilarity after noise regions are discounted.

Figure 5.3 shows the distribution of the Hamming distance when our segmentation algorithm is used. Figure 5.4 shows the distribution of the Hamming distance when Daugman segmentation algorithm is used. The results show that the match distribution when our algorithm was used has shifted a significant distance to the left. The mean of the match distribution has decreased by 0.12. In Figure 5.4, the distance between the two means equals 0.075, and the distance between the two means in Figure 5.3 equals 0.19. We notice that the distance between the match and non-match distribution is increased,

because the proposed segmentation algorithm is used, as a result the error rates will be decreased and a large improvement over Daugman algorithm performance is achieved.

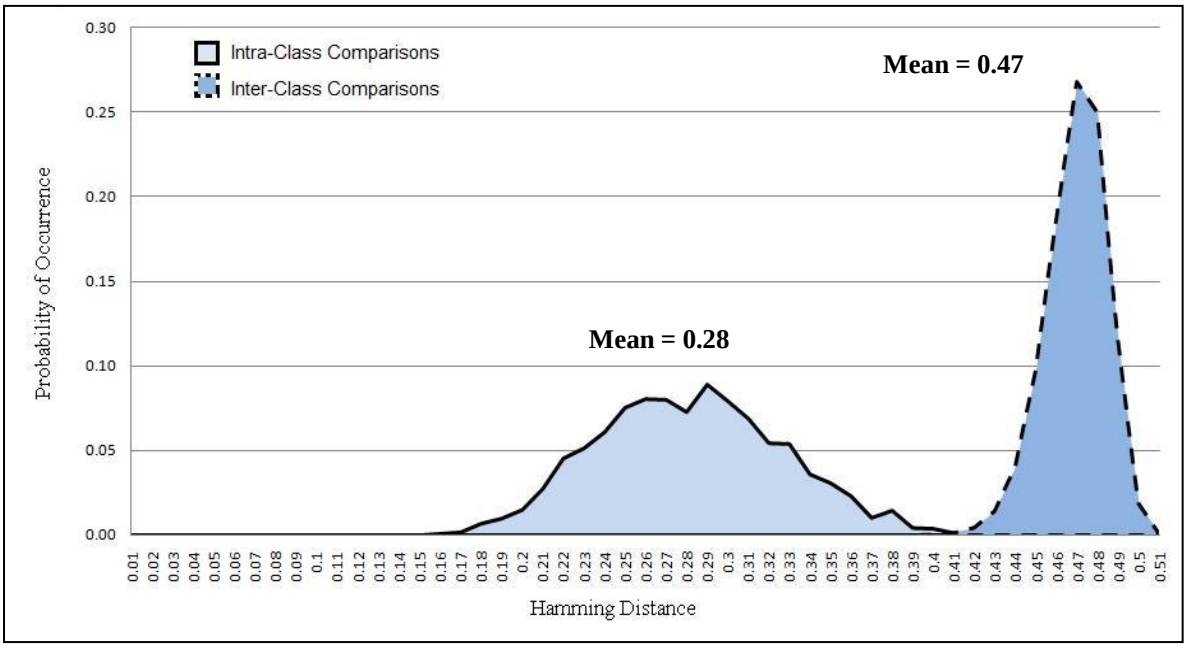

Figure 5.3: The match and non-match distributions for UBIRIS v1 when our segmentation algorithm is used.

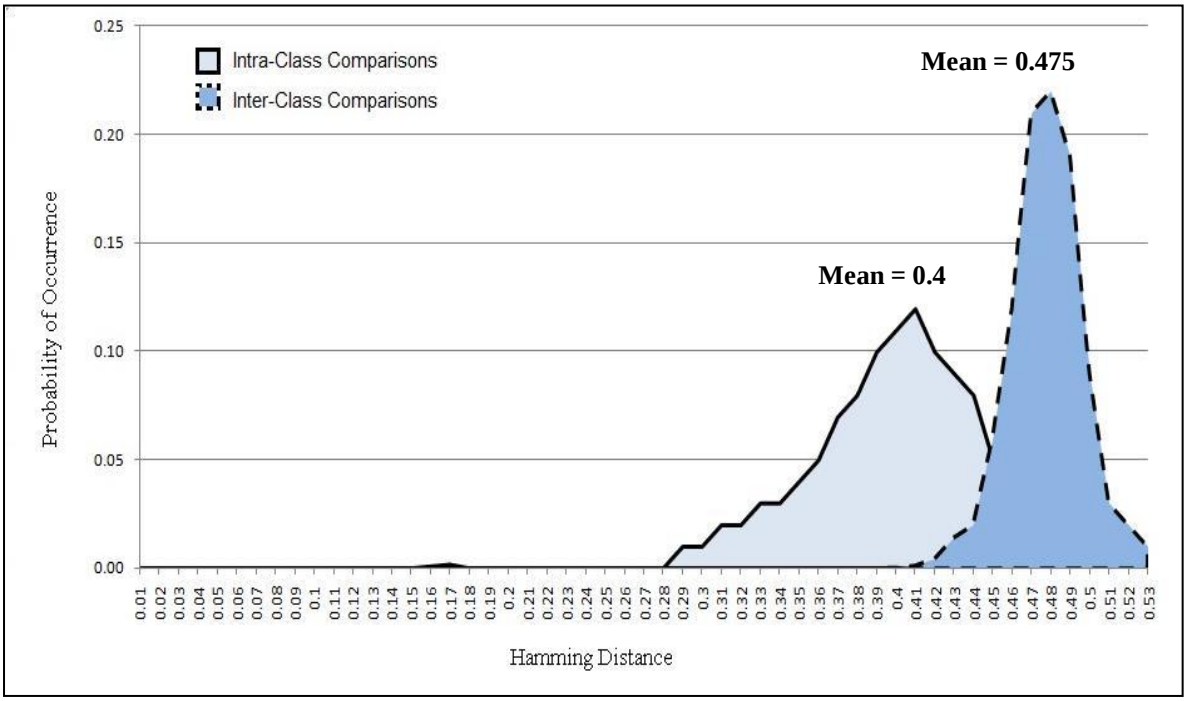

Figure 5.4: The match and non-match distributions for UBIRIS v1 when Daugman algorithm is used.

Also, it is noted that when the proposed segmentation algorithm is used, the interference of the match and non-match distribution is less than when Daugman segmentation algorithm is used. This is because the Daugman segmentation algorithm is very sensitive to noise and could not handle noise factors which occurred in non-ideal conditions such as specular reflections, pupil isolation and eyelids occlusion.

Figure 5.5 shows the EER of iris recognition system when our proposed algorithm is used. EER is the point at which FMR and FNMR are almost equal. EER enables evaluation of FMR and FNMR at a single operating point. The EER is very low, when the proposed segmentation algorithm is used comparing with EER of the iris recognition system when Daugman segmentation algorithm is used. This result shows that the proposed segmentation algorithm accurately isolate error regions in iris template. And so, the FMR and FNMR will decrease. Daugman segmentation algorithm could not handle these sources of error, because its designed to work in ideal conditions, and use the Integro-Differential operator which frequently fails when the images do not have sufficient intensity separability between the iris and the sclera.

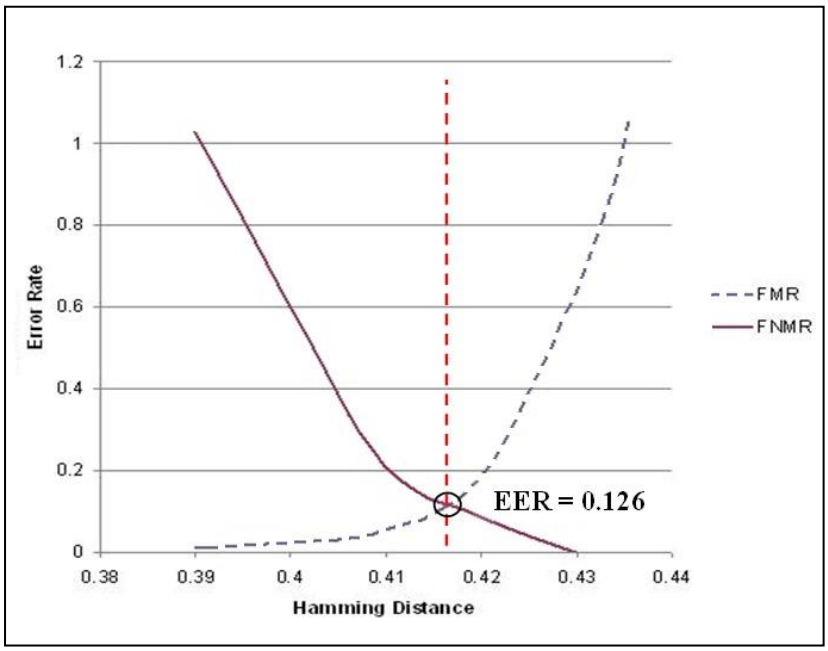

Figure 5.5: The Equal Error Rate value where FMR and FNMR are equal.

To evaluate the performance of the proposed segmentation algorithm over different techniques, Daugman's method is implemented using some functions from Masek's iris

recognition algorithm [71], and results described in [73] is used. We use the most important points to compare our algorithm with others, which is FAR(%) at 0.0001% FRR and FRR(%) at 0.0001% FAR. The experimental results on the three algorithms are summarized in Table 5.2. In this table, it is shown that the proposed segmentation algorithm significantly reduces the two metric values. As we said before, the good performance of our segmentation algorithm is due to its ability to handle any source of error type, which might occurs in non-ideal enviroments.

Table 5.2: Comparison of the proposed algorithm with two previous algorithms.

Method	**FAR(%) at 0.0001% FRR**	**FRR(%) at 0.0001% FAR**
Daugman	7.2	12.96
SVM Match Score Fusion	5.9	8.71
Proposed	1.5	5.82

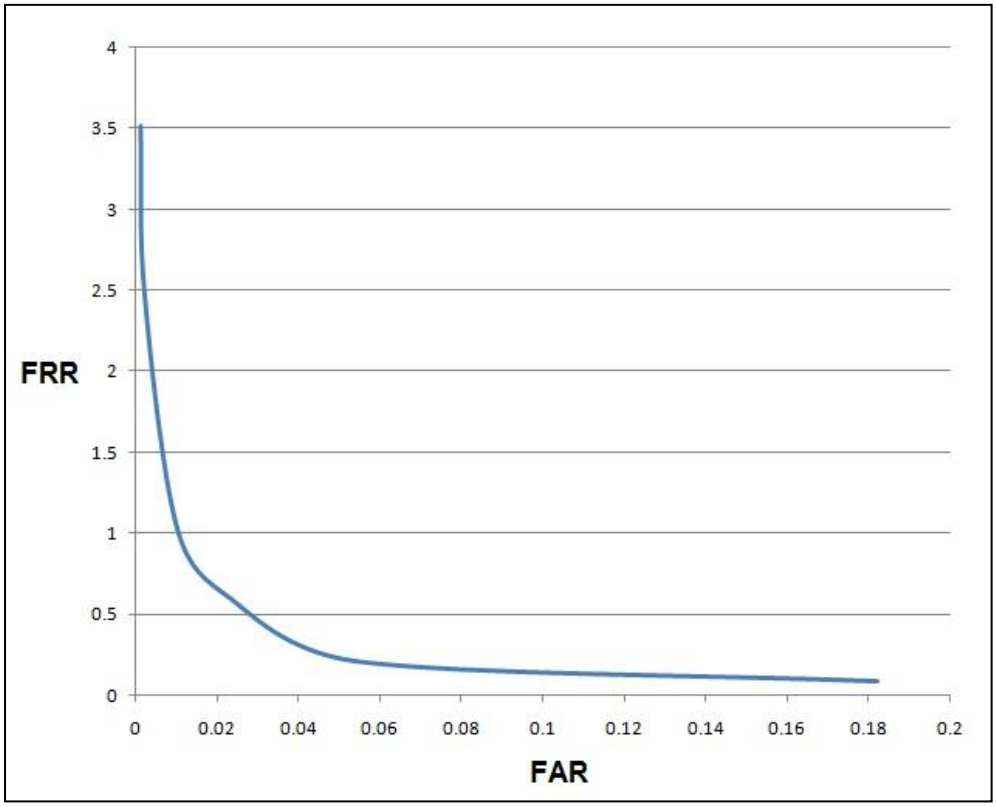

Figure 5.6: ROC curve, reflecting the relation between the FAR and FRR.

Figure 5.6 shows the ROC curve when our proposed segmentation algorithm is used. We can see from this figure that the FAR and FRR approximately equal in 0.16, which is a very low value. On the other hand, FRR increases faster than FAR, this will not affect the iris recognition system very much because the most important value in security is FAR. As mentioned in Section 1.4, the FRR and FAR can be adjusted in a way that reflects their associated costs and benefits. This depends on the application which the iris recognition system will be used in.

5.4 Results of Pupil Dilation

5.4.1 Dataset

In the pupil dilation experiments, we use CASIA-IrisV3 [69] as described in Section 5.1. We did not use the whole images of this database because many iris images are not very affected by turning the lamp on/off close to the subject. As a result, many images have approximately the same pupil dilation degree for the same class which will not help in our research. Therefore, 721 images for 41 persons is selected from the CASIA-IrisV3-Lamp database. The selected dataset contains the best images in the database which have a high variation in pupil dilation degrees for the same class, and at the same time the iris region is not affected by different types of noise (Poor focused, Motion blurred, Iris obstructions due to eyelashes, Iris obstructions due to eyelids, Iris with specular reflections …). Therefore, the selected dataset is affected by only one type of noise which is the differences in pupil dilation degrees. Figure 5.7 shows the high variation in pupil dilation degrees of three classes from our selected dataset.

Pupil dilation degree is computed by obtaining the radius of the pupil and the radius of the iris. So, firstly we need to localize and segment each iris in our dataset then the radius of iris and pupil is obtained. All the dataset' irises are true segmented because it is selected carefully, and if any iris has an inaccuracy in its segmentation, we exclude it from the dataset in the selection stage as said before to make our dataset has only one problem or source of error it’s the pupil dilation.

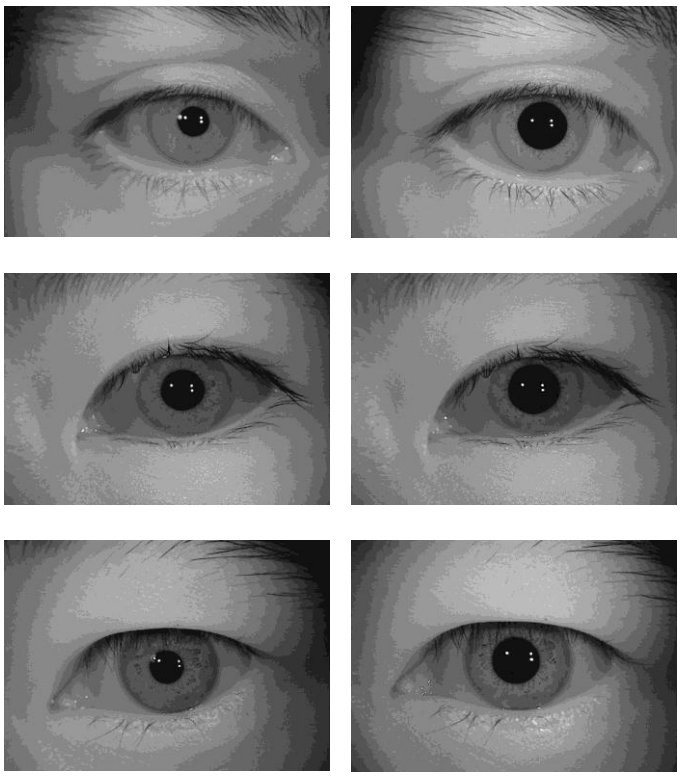

Figure 5.7: The big difference of pupil size in our selected dataset.

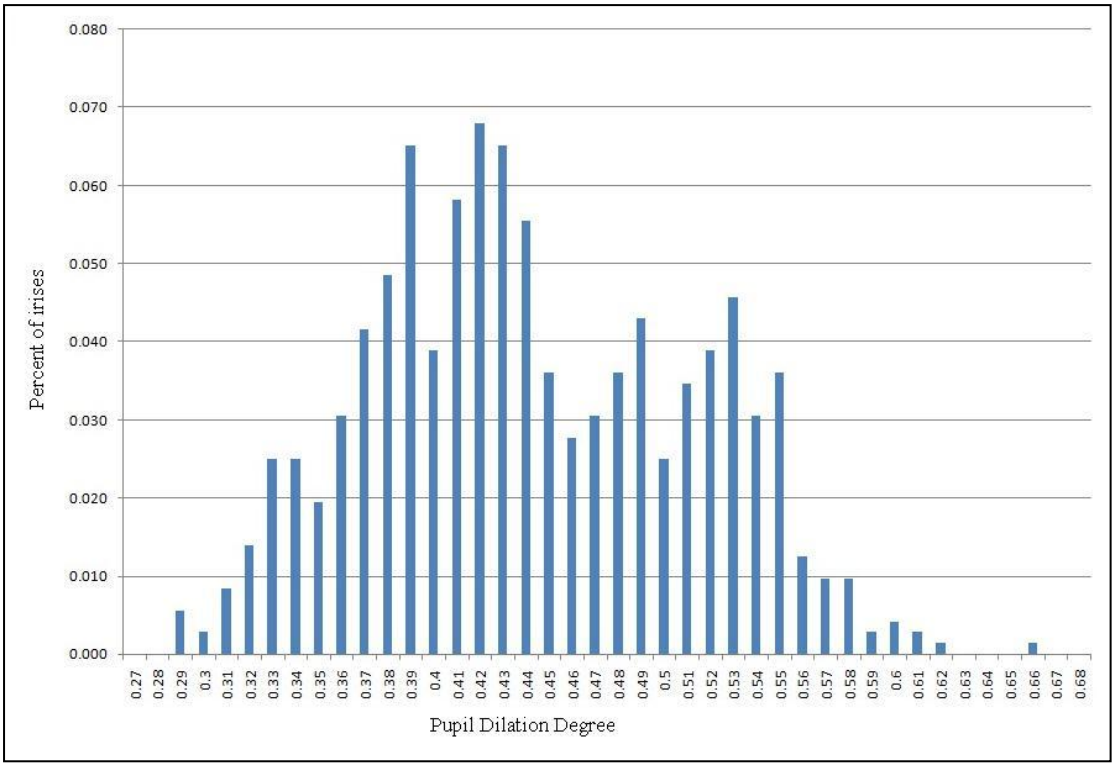

Figure 5.8: Pupil dilation ratios in our dataset.

To measure dilation, we use a simple method used by many researchers [28]. This process measures the degree of dilation by dividing the pupil radius on the iris' radius. Since the pupil radius is always less than the iris' radius, this dilation ratio must fall between 0 and 1. In the selected 721 images, all dilation ratios were between 0.28 and 0.66. The distribution of dilation ratios is shown in Figure 5.8. It is observed that the datasets have widely variations in pupil dilation degrees, which will be necessary in evaluating the effect of dilation in a good and fair experiments.

5.4.2 The Effect of Pupil Dilation on Performance

To show that the pupil dilation affects the performance of iris recognition system, all irises in our dataset is first segmented using circular Hough transform to detecting the iris and pupil boundaries. This involves first employing Canny edge detection to generate an edge map. Gradients were biased in the vertical direction for the outer iris/sclera boundary, as suggested by Wildes et al. [74]. In cases the segmentation software detect occlusion by eyelids, parts of the iris region are masked (Figure 5.9). This can limit the effect of eyelids and eyelashes on the results.

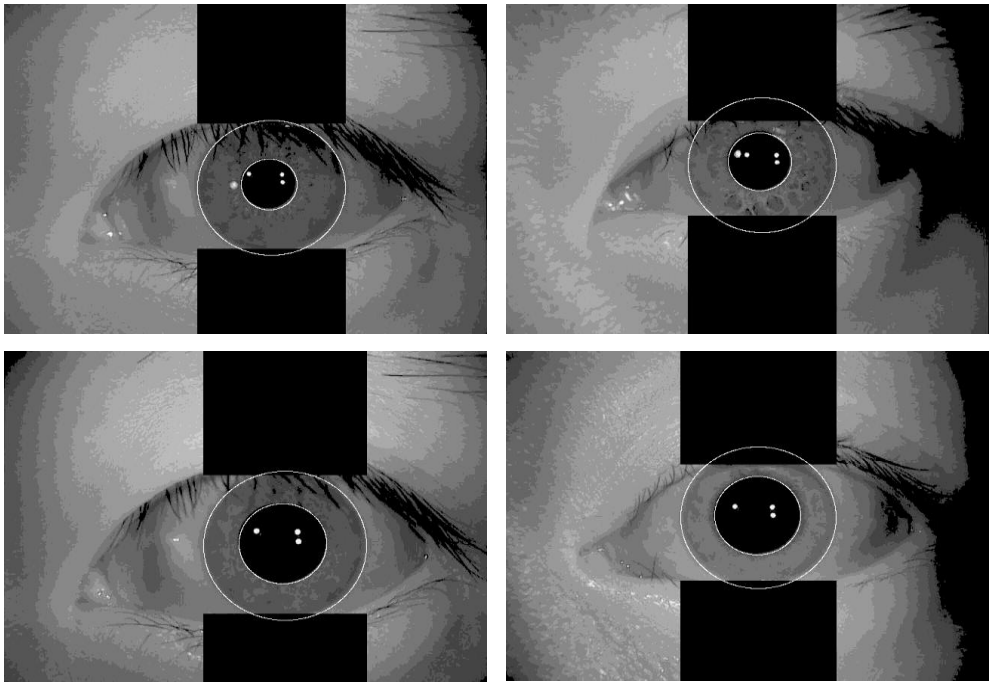

Figure 5.9: Samples of segmented and masked noise irises from our selected dataset.

After that, the segmented irises are normalized using Daugman approach. In the feature encoding step, we convolve the normalized iris patterns with 1D Log-Gabor wavelets [75] to generate 2x20x240 bit iris template for each iris. The available MATLAB code of Masek [71] is used. We divide the irises into two groups, irises with pupil dilation degrees less than 0.5, and irises with pupil dilation degrees more than or equal 0.5. Then, we compare each iris template in the dataset with the other iris' templates in two cases. When use all images, and when excludes irises in the second group (dilation degree more than 0.5).

In the first experiment, the compared iris images equal 721. The total number of comparisons equals 259,731 where the total number of intra-class comparisons equals 6270 and that of the inter-class comparisons equals 253,461. In the comparison stage, we use the HD as the metric of dissimilarity between two considered iris' codes.

In the second experiment, the compared iris images equal 555, after excluding 166 images which have pupil dilation degrees more than 0.5. Table 5.3 shows the result of each experiment. It is clearly observed that when irises with high pupil degree excludes from the dataset, the FMR and FNMR are reduced and the percent of true match and true non-match are increased. This means that irises with high pupil dilation degrees cause more errors in iris' templates. Figure 5.10 and Figure 5.11 show the match and non-match distributions for the first and second experiment respectively.

Table 5.3: Comparison of results when using all irises and when using irises with pupil dilation degree less than 0.5.

Performance value	All irises in our dataset	Irises with pupil dilation degree less than 0.5
False Match Rate	0.027%	0.004%
False Non Match Rate	1.39%	0.69%
True Match Rate	99.973%	99.996%
True Non Match Rate	98.61%	99.31%

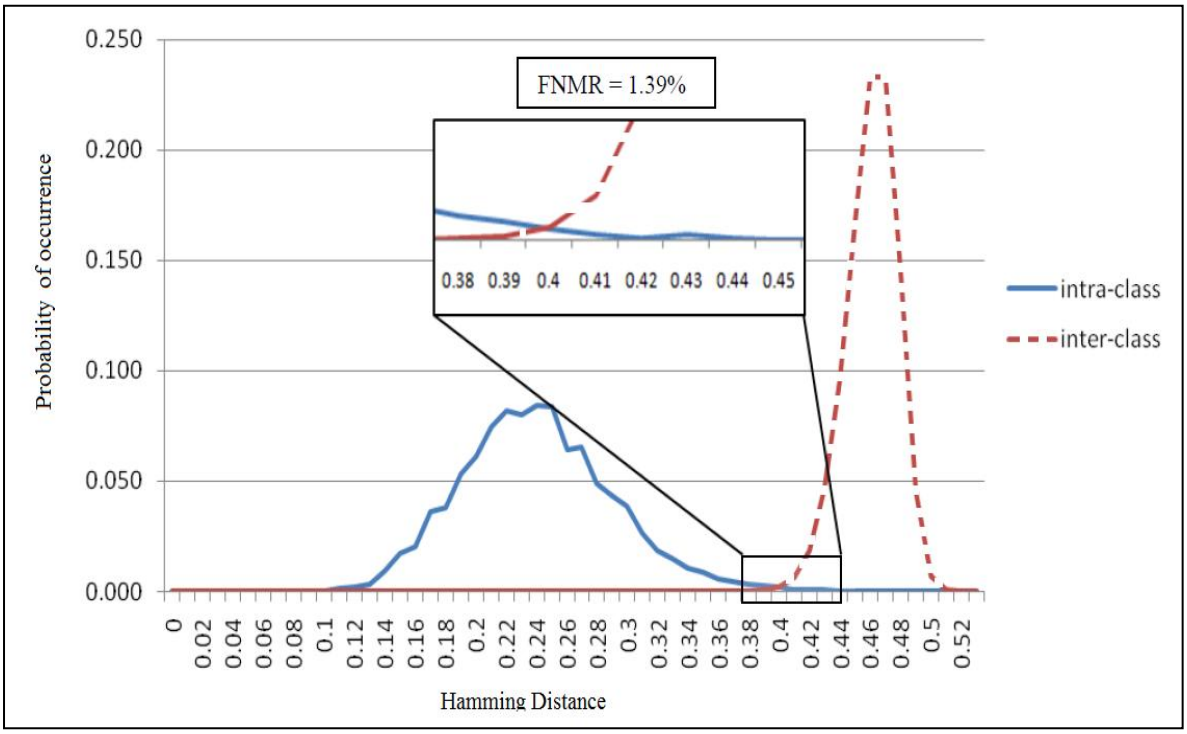

Figure 5.10: The match and non-match distributions for our selected dataset when all images are used.

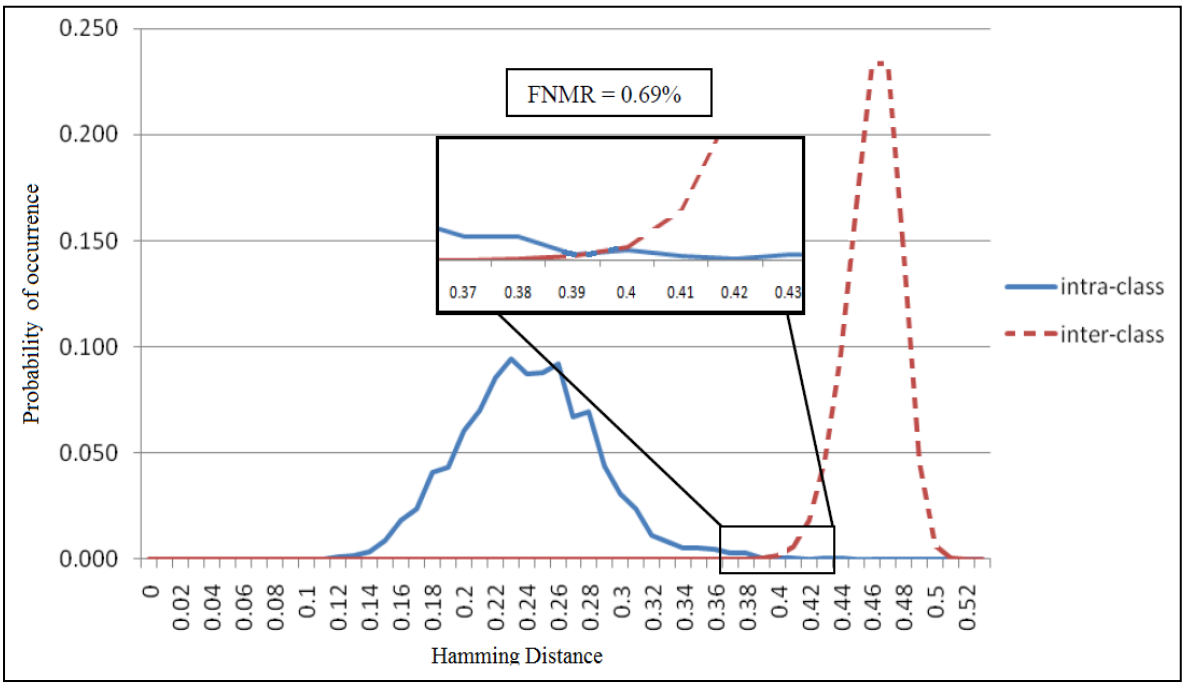

Figure 5.11: The match and non-match distributions for our selected dataset when images with pupil dilation degree <= 0.5 are used.

As we can see from the previous two figures, the FNMR decreases when we use non-dilated pupil from 1.39% to 0.69%. At the same time, the true match rate is increased to 99.996% which is a very good value. This means that pupil dilation affects the identification and recognition processes by degrading some iris' bits in iris' code. This error is caused by the assumption that when the pupil dilates, the stretch of the iris tissue in the radial direction is linear during the normalization process. So, the normalization of the iris causes some errors when comparing two images of different sizes, if the stretch of the iris is non linear. It is noticed that all irises stretch in linear direction when its pupil dilated, also not all irises have non-linear stretch when their pupil dilated.

The behavior of dilation depends on many factors like the color of the eyes, the health of eyes and the age of the person. Therefore we could not accurately predict deformations of the iris when the pupil dilates. Some researchers try to enhance the performance of recognition system in cases where the irises with dilated pupils are used to estimate the parameters of the relative deformation between a pair of images [76] or to modeling nonlinear iris stretch as a sum of linear stretch, and a Gaussian deviation term [55]. But as we explained before, these algorithms did not solve the problem completely. Our idea is to prevent the high pupil dilation (which cause errors in iris code) from occurring during capturing iris images in iris recognition system rather than trying to handle it. In other word, the important question that will be asked is : what is the highest pupil dilation degree that can be accepted by the recognition system, while maintaining the high accuracy in its performance? The next section tries to answer this question.

5.4.3 The Limit of Pupil Dilation

Many researchers try to test the effect of pupil dilation on iris template, and to study how different degrees of pupil dilation affect the performance of an iris' biometric system. No prior work has quantified: what is the degree of pupil dilation if the dilation exceeds it, the performance of an iris biometric system will be affected. In other words, we will find the pupil dilation limit that the pupil dilation in the iris should not exceeds it, to get the best results. In the following experiment, irises with high degree of pupil dilation will be excluded gradually from the selected dataset and in each case all irises in the dataset are

segmented using circular Hough transform and edge detection. Then, we mask the noise regions (e.g. eyelashes, eyelids and reflections) using masks (see Figure 5.9). After that, we normalize and encode all irises to generate 2x20x480 bit iris' template using the same methods used in Section 5.3.2 for each iris.

After generating all the templates of all irises, we compare each iris template in the database with all the other iris templates in the database using the Hamming distance as the metric of dissimilarity between two considered iris codes to get the match and non-match distributions for selected dataset, when images with pupil dilation degree <= P_{deg} . where P_{deg} is the degree of pupil dilation which irises with pupil dilation degree more than it, will be excluded from the dataset. P_{deg} will start from 0.66 (the high value of pupil dilation) and decreased gradually (0.61, 0.59, 0.58 ….). This means that in each step, the most dilated pupils are excluded from the dataset, and then we compute the FNMR error to evaluate the effect of excluded irises on the dataset. Figure 5.12 shows the result.

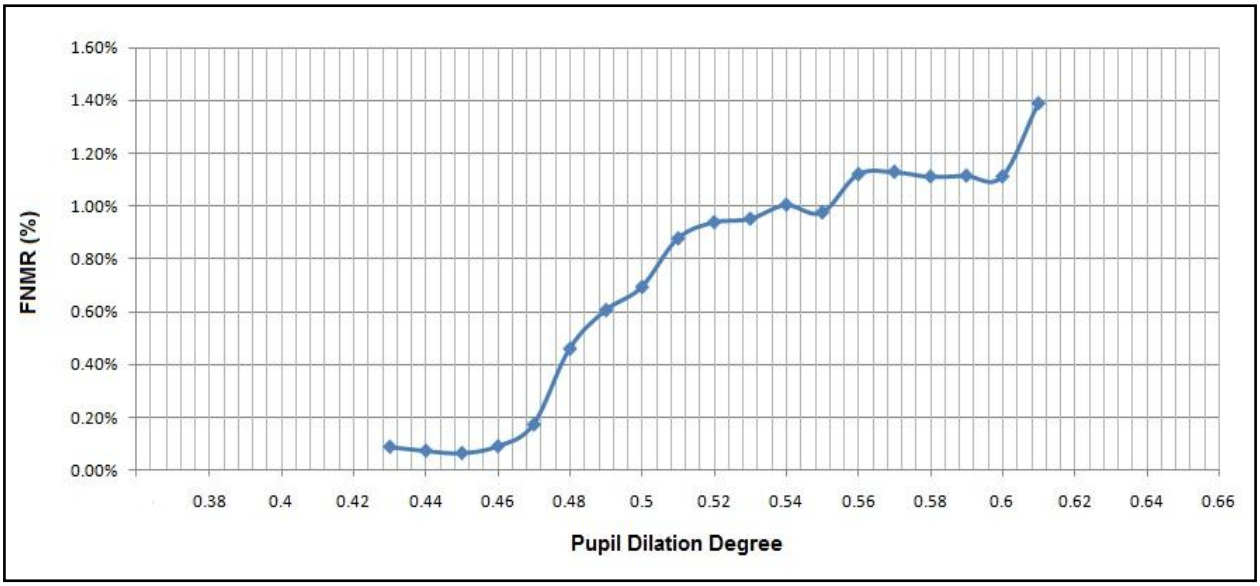

Figure 5.12: The FNMR when gradually delete irises with high pupil dilation degree.

As shown in Figure 5.12, the minima in the graph occurs when pupil dilation degree equals 0.45, then the FNMR equals 0.07% and the TNMR = 99.93%. Before and after 0.45, the FNMR increase. The FNMR has the highest value, when all images in the

dataset is used in analysis without excluding any dilated pupil template. We notice that the error value decreases as we exclude more dilated pupil templates from the dataset, until we reach the pupil dilation degree of 0.45. When we begin excluding templates with pupil dilation equal 0.44 and 0.43, the FNMR begins increasing again. We notice that when excluding this group of templates, the error remains as it is, but the true non-match rate is decreased. This means that the remaining error is not caused by the pupil dilation. As a result, we recommend that to obtain a strong secure iris recognition system, the degree of dilation for any pupil must be less than 0.45. If pupil dilation degree is more than 0.45, we can use one of the previous proposed algorithms to handle pupil dilation. Figure 5.13 shows the match and non-match distributions of our selected dataset when images with pupil dilation degree <= 0.45 are used. We note that the FNMR error is reduced to 0.07.

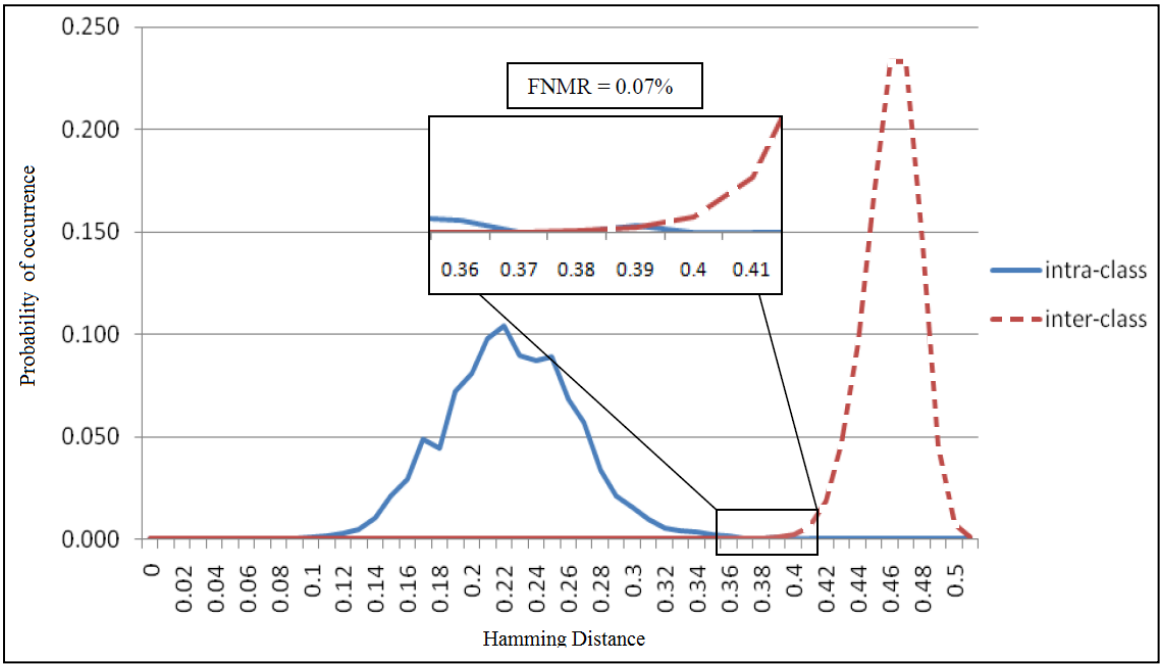

Figure 5.13: The match and non-match distributions for our selected dataset when images with pupil dilation degree <= 0.45 are used.

5.5 Analyzing Iris Code Bits

5.5.1 Dataset

CASIA-Iris-Interval [10] is selected to be used in this experiment. To study the inconsistent bits in irises we select 310 images from 22 persons (160 image for the left eye and 150 image for the right eye). The best images from the CASIA-Iris-Interval database are selected which have high detailed texture and the iris region did not affected by different types of noise (Poor focused, Motion blurred, Iris obstructions due to eyelashes, Iris obstructions due to eyelids, Iris with specular reflections …) . All irises in the dataset are segmented to find correct inner and outer boundaries of the iris using circular Hough transform and then the noise regions are masked in cases where the segmentation software detects occlusion caused by eyelids in order to minimize the effects of segmentation errors. Then, all segmented irises are normalized and encoded to generate 2x20x240 bit iris' template for every iris using 1D log-Gabor wavelets. Figure 5.14 shows samples of segmented irises of our selected dataset from CASIA-Iris-Interval database.

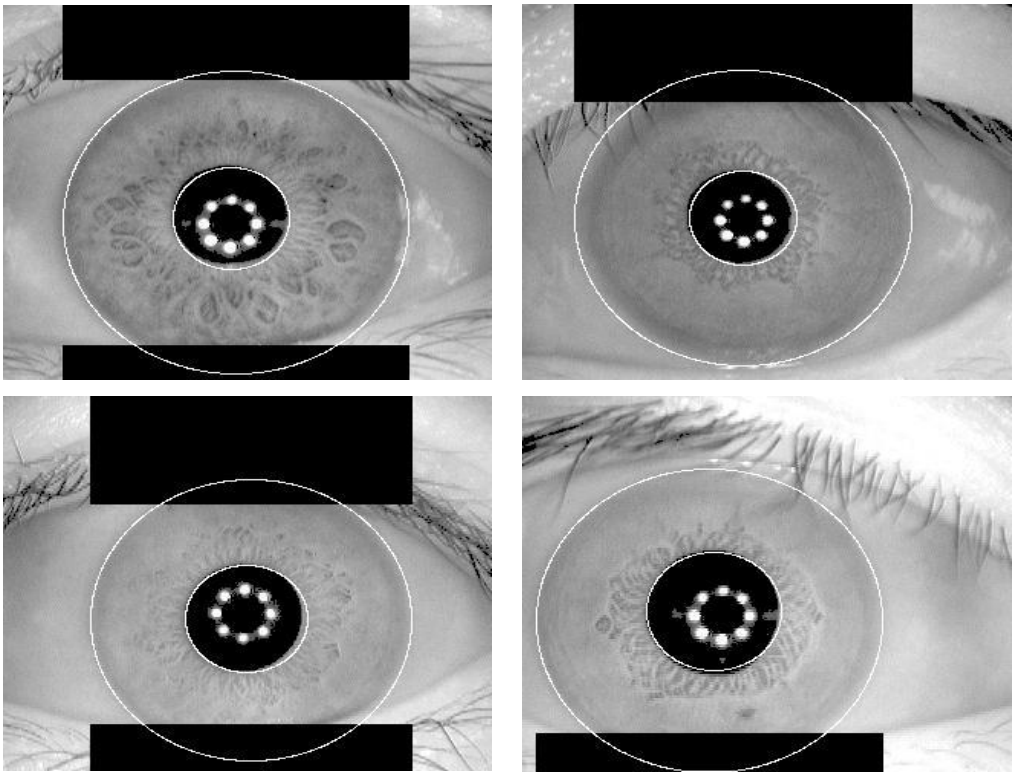

Figure 5.14: Samples of segmented irises from our selected dataset from CASIA-Iris-Interval database.

Each iris' template in the dataset is compared with all the other iris' templates in the dataset using the Hamming distance as the metric of dissimilarity between two considered iris' codes. The result of this experiment is shown in Table 5.4. The FMR and FNMR errors are very small because we mask all noises and selecting iris images carefully. This is important to concentrate the analysis on the fragile bits.

Table 5.4: Error Rates of our selected dataset from CASIA-Iris-Interval.

Type	Rate
False Non Match Rate (FNMR)	0.212%
True Non Match Rate (TNMR)	99.788%
False Match Rate (FMR)	0.020%
True Match Rate (TMR)	99.980%

5.5.2 Inconsistent Bits

To investigate the existence of inconsistent bits in our selected dataset, we generate the templates and the masks for each iris as shown in Figure 5.15. The real part and the imaginary part of each iris template are quantized to 0/1, giving two bits of iris code for each texture filter result. Thus, the system used here generates an iris code that is 2 x 20 x 240 = 9600 bits. The masks is 20x240 bits. Then, the templates and the masks of the irises of the same person are compared to determine which bit is consistent (keep its bit value for more than 80% of images) or inconsistent (its bit value changed for more than 20% of images). Figure 5.16 shows the result of comparing templates and masks for three persons. real part (20x240 bit) and imaginary part (20x240 bit) are separated to view the results in more details. White bits present the consistent bits while, black bits represent the inconsistent bits. The two black domes below the two rectangles are the masked region. We notice that the inner parts of iris code are better and more consistent than the outer parts.

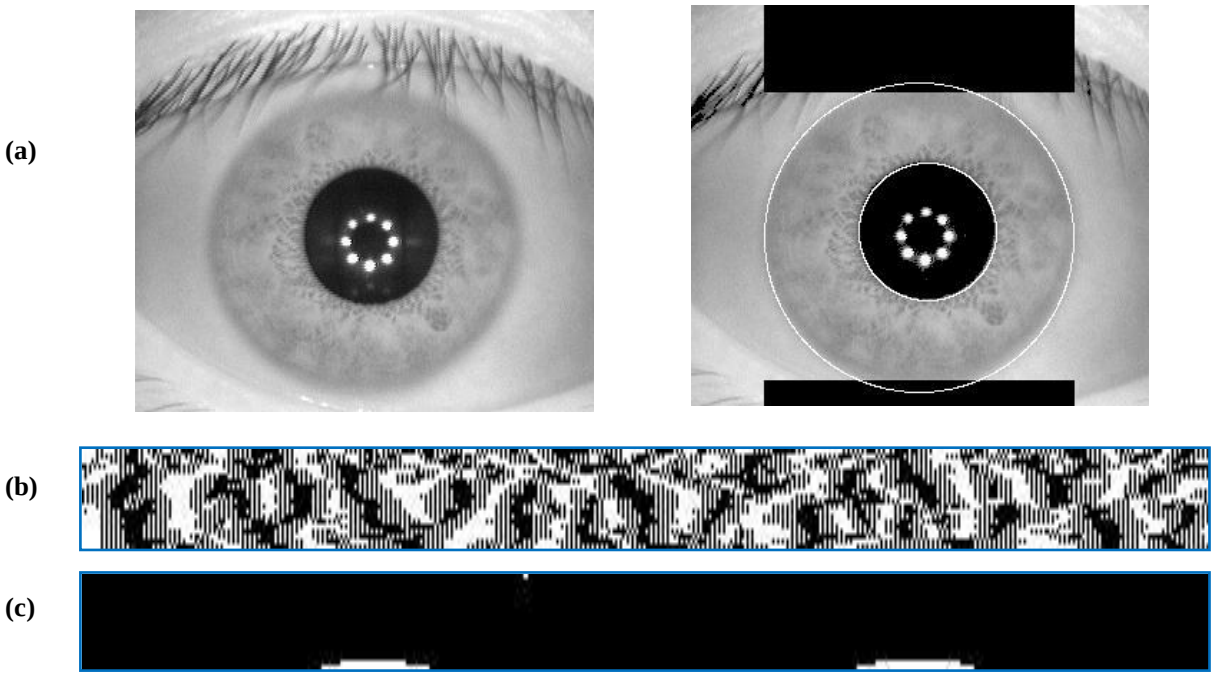

Figure 5.15: Sample of segmented and encoded iris from our selected dataset from CASIA-Iris-Interval database.(a) iris image before and after the segmentation. (b) iris template. (c) iris mask.

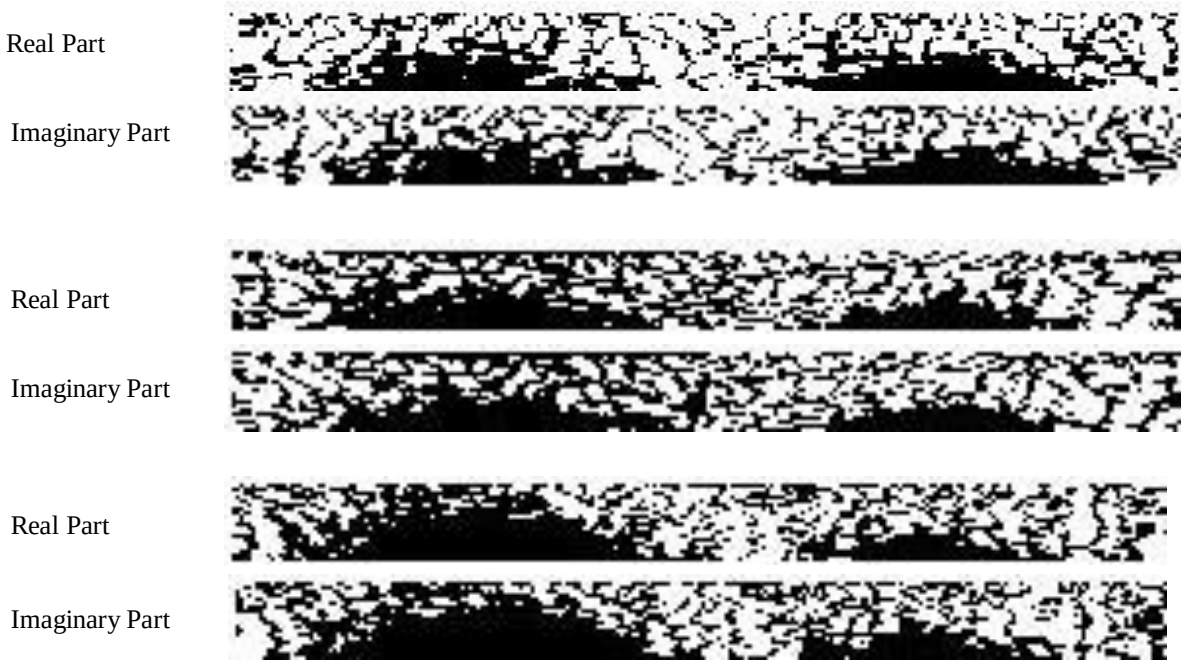

Figure 5.16: Result of comparing templates and masks for three persons.

In this experiment, it is found that 44.3% of the bits of iris' code in the dataset are consistent, while 55.7% of the bits is inconsistent or occluded by eyelashes and eyelids. This means that approximately the half of iris code bits are inconsistent or can be dropped or excluded from the iris code. The maximum percentage of consistent bits for one class in our dataset is 64.8% and the minimum percentage equals 15.3%. It is observed that classes with low degree of consistent bits are found in three cases :

1. When there is a small error in segmentation, because the non-circular shape of the pupil. This lead to fragile many bits in iris' codes as shown in Figure 5.17.
2. When there is more pupil dilation variation in the same person irises. This can fragile many bits in the iris' code.
3. The normal noise like unmasked luminance, reflections and unmasked eyelashes in iris' code.

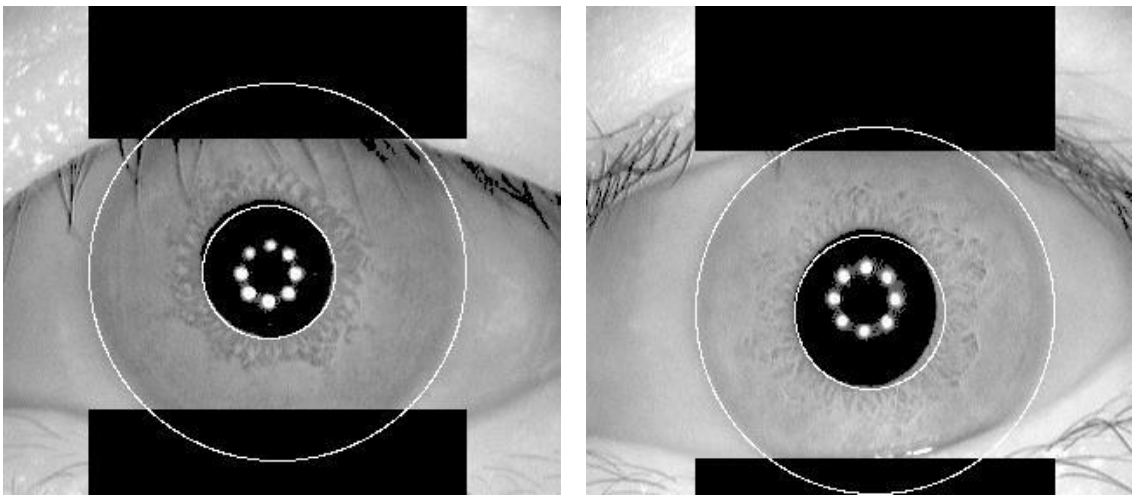

Figure 5.17: Samples of segmented irises from our selected dataset that have many inconsistent bits because the wrong segmentation due to non-circular shape of the pupil.

5.5.3 The Best Parts of Iris Code

To determine the best regions in iris' code, the iris code is divided into four parts, each part is 5x480 bits as in Figure 5.18. We mask each part separately and execute the matching test as performed in the previous experiment, and we compute the FNMR for each one. Table 5.5 shows the result of masking each part separately. It is observed that

the best two regions (the regions which will affect the performance when they are masked are the inner regions, the second and the third) because the error rate will be slightly bigger than when the two outer regions are masked.

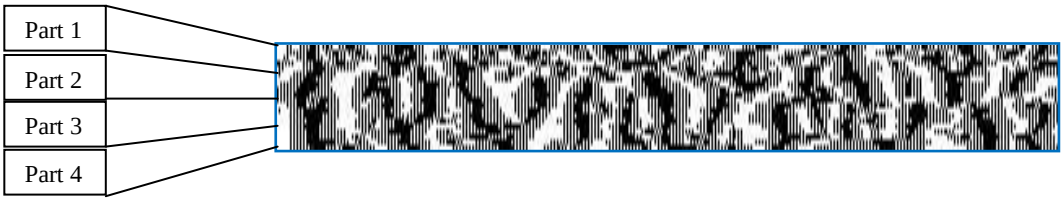

Figure 5.18: Four parts of iris code that we use to compare the performance of each part.

This result is due to that the outer two sectors contain many types of errors, for example the outer sector near the pupil might be affected by non-circular pupil problems, where the outer sector near the sclera might be affected by eyelashes and eyelids problems.

Table 5.5: Comparison of FNMR when each of the four parts of the iris are masked.

Masked Region	FNMR
Part 1 (1-5)	0.146%
Part 2 (6-10)	0.219%
Part 3 (11-15)	0.220%
Part 4 (16-20)	0.15%

To test the effect of using the inner sectors on the hole system, we segment all irises of the dataset using circular Hough transform and Canny edge detection to detecting the iris and pupil boundaries. We normalize the segmented irises using Daugman rubber sheet model using the inner two sectors only. Then all normalized irises are encoded using Log-Gabor filter to generate the real and imaginary parts of iris code for each iris. Every iris code is 2 x 20 x 240 bit. To compute the match and non-match distributions for this dataset, each iris image in the database are compared with all other irises in the database. So, there are two comparisons groups, intra-class comparisons and inter-class comparisons. During the comparison stage, the HD is used as the metric of dissimilarity

between two considered iris' codes. After computing the match and non-match distributions for this dataset, the FMR and FNMR errors are computed. Table 5.6

Table 5.6: Comparison of results when using all iris code bits and when using the two inner sectors only.

Performance value	when using all iris code bits	when using the inner two sectors
False Match Rate	0.020%	0.019%
False Non Match Rate	0.212%	0.144%
True Match Rate	99.980%	99.981%
True Non Match Rate	99.788%	99.856 %

It is clearly observed that when using the inner two sectors of iris code in computing the match and non-match distributions for the dataset, the FMR and FNMR are reduced and the percent of true match and true non-match are increased. This means that the bits in the outer two sectors contain more errors causes than the inner sectors in iris' templates, and as a result the performance of the iris biometric system will increase.

As we can see from the previous table, the FNMR decreases when we use only the inner sectors of the iris template from 0.212% to 0.144 %. At the same time, the FMR is decreased slightly from 0.020 to 0.019%. This means that we can use the inner sectors of iris template in the identification and recognition processes to reduce the errors and to avoid many inconsistent bits in the outer sectors of iris' bits in iris' code.

Chapter 6

Conclusion

6.1 Summary and Concluding Remarks

This research proposes new algorithms to solve two problems in iris recognition system, segmenting irises in non-ideal environments and pupil dilation. At the last, the bits of the iris code are analyzed. First, a new effective and fast segmentation algorithm is proposed to segment the non-ideal iris images captured with less constraining imaging conditions which will generate several types of noises, such as iris obstructions, poor focused and off-angle iris images. The proposed algorithm adds a new pre-processing step to segmentation process by clustering the iris image first using simple K-means algorithm. This can exclude the non-iris regions which causes many errors, and decreases the searching time in the next steps. Circular Hough transform is applied to the binary edge map for the estimated iris region (result from clustering algorithm) to localize the outer iris borders. To reduce the computational time of CHT, the scale of image is reduced to the half and the edge point are reduced by executing vertical edge detection only. A new method to localize the upper eyelids is proposed by detecting it in the sclera region. This is because the intensity contrast of sclera and upper eyelid are very high comparing with the intensity contrast of iris and eyelid. To localize the lower eyelid of the iris line Hough transform is used, because the most of the occlusions of the lower eyelid is approximately linear. Specular reflection is removed using advanced variable intensity limit. Finally, in order to remove the pupil region using CHT, iris image is adjusted by mapping its bits intensity values to new values to focus on dark intensities. Experimental results on UBIRIS V1 iris database indicate the high accuracy and faster execution of our segmentation algorithm comparing with previous algorithms.

Second, the pupil dilation problem is discussed, and its effects on the iris recognition system are analyzed. We select a good dataset irises with a high pupil dilation degree variations from CASIA-IrisV3 database. In the first experiment, it is observed that the pupil dilation affects the performance of iris recognition by increasing the FMR and

FNMR error values. This result is due to the stretch of the iris when pupil dilation occurs is non linear and depends on many factors. So, we can not estimate a model to handle this problem completely. In the second experiment, we determine experimentally the degree of pupil dilation if the pupil dilation exceeds it, the performance of an iris biometrics system will be affected. This means that the pupil dilation would not affect the performance of recognition system as soon as its degree is less than the estimated limit determined in this thesis. So, to obtain a strong and secure iris recognition system we recommend that the degree dilation for any pupil must be less than 0.45.

Finally, the iris code bits is analyzed using selected dataset contains 310 images from 22 persons. 160 images for left eye and 150 images for right eye. The best images from the CASIA-Iris-Interval database are selected which have high detailed texture and the iris region is not affected by different types of noise. The iris code template of each image is generated then we compare templates and masks of irises for the same person to determine which bits are consistent (keep its bit value for more than 80% of images) or inconsistent (the bits value are changed for more than 20% of images). It is observed that 44.3% of the bits of the iris code in our dataset are consistent while 55.7% of the bits are inconsistent. This means that we can exclude the half of the bits of the iris code. In the second experiment, the iris code is divided into four sectors and we found that the best two sectors are the inners, which are the second and the third sectors, but the difference between the four sectors are not very large.

6.2 Future Work

Researches in the area of iris recognition systems are growing fast. Due to the continues spreading of using iris recognition system in several applications. The current work focuses on segmentation and normalization stages. Future research work will be first focused on developing our proposed algorithms in this thesis by implementing the algorithms using C++ programming language. This will increase the performance of the algorithms and make it faster.

In the other hand, there are some new research ideas related to our thesis work needs to be tested and analyzed. The following points view these ideas.

- Enhancing the encoding stage to be suitable to iris images captured in non-ideal conditions.
- Finding the best encoding methods that can handle different types of errors such as pupil dilation.
- Studying the effect of pupil dilation on the iris code using the concepts of consistent and inconsistent bits.

References

[1] A. Jain, R. Bolle, and S. Pankanti, "Biometrics: Personal Identification in a Networked Society," Norwell, MA: Kluwer, 1999.

[2] D. Zhang, "Automated Biometrics: Technologies and Systems," Norwell, MA: Kluwer, 2000.

[3] J. Daugman, "Statistical richness of visual phase information: update on recognizing persons by iris patterns," *Int. J. Comput. Vis.*, vol. 45, no. 1, pp. 25–38, 2001.

[4] J. Daugman, "Demodulation by complex-valued wavelets for stochastic pattern recognition," *Int. J.Wavelets, Multi-Res. and Info. Processing*, vol. 1, no. 1, pp. 1–17, 2003.

[5] R. Wildes, "Iris recognition: an emerging biometric technology," *Proc. IEEE*, vol. 85, pp. 1348–1363, Sept. 1997.

[6] J. Daugman, "How iris recognition works," *IEEE Transactions on Circuits and Systems for Video Technology*, 21–30 2004.

[7] L. Flom and A. Safir, U.S. Patent 4 641 394, 1987. "Iris Recognition system" .

[8] J. Daugman, U.S. Patent 5 291 560, 1994. "Biometric personal identification system based on iris analysis".

[9] J. Daugman, "High confidence visual recognition of persons by a test of statistical independence," *IEEE Trans. Pattern Analy. Machine Intell.*, vol. 15, pp. 1148–1161, Nov. 1993.

[10] http://biometrics.idealtest.org/dbDetailForUser.do?id=4.

[11] J. Daugman, "Demodulation by complex-valued wavelets for stochastic pattern recognition," *Int. J.Wavelets, Multi-Res. and Info. Processing*, vol. 1, no. 1, pp. 1–17, 2003.

[12] W. Boles and B. Boashash, "A human identification technique using images of the iris and wavelet transform," *IEEE Trans. Signal Processing*, vol. 46, pp. 1185–1188, Apr. 1998.

[13] Y. Zhu, T. Tan, and Y. Wang, "Biometric personal identification based on iris patterns," in *Proc. Int. Conf. Pattern Recognition*, vol. II, pp. 805–808, Nov, 2000.

[14] C. Park, J. Lee, M. Smith, and K. Park, "Iris-based personal authentication using a normalized directional energy feature," in *Proc. 4th Int. Conf. Audio- and Video-Based Biometric Person Authentication*, pp. 224–232, Jun. 2003

[15] K. Bae, S. Noh, and J. Kim, “Iris feature extraction using independent component analysis,” in *Proc. 4th Int. Conf. Audio- and Video-Based Biometric Person Authentication*, pp. 838–844, Jun. 2003

[16] Wikipedia, the free encyclopedia. http://en.wikipedia.org/wiki/Biometrics.

[17] WhatIs Dictionary. IT encyclopedia and learning center, 2005. http://whatis. techtarget.com/.

[18] Jain, A. K.; Ross, Arun; Prabhakar, Salil (January 2004). "An introduction to biometric recognition," IEEE Transactions on Circuits and Systems for Video Technology 14th (1): 4–20.

[19] Hugo Proenca. Towards Non-Cooperative Biometric Iris Recognition. PhD thesis, University of Beira Interior, October 2006.

[20] K. Delac and M. Grgic, "A survey of biometric recognition methods," In Proceedings of the 46th International Symposium Electronics in Marine (ELMAR-2004), pages 184–193, Croatia, June 2004.

[21] W. Zhao, R. Chellappa, P. J. Phillips, and A. Rosenfeld, "Face recognition: A literature survey," ACM Computing Surveys, vol. 35, issue 4, pages 399–458, December 2003.

[22] P. J. Philips, P. Grother, R. J. Micheals, D. M. Blackburn, E. Tabassi, and J. M. Bone. Frvt2002: Overview and summary, 2002. http://www.frvt.org/FRVT2002/ documents.htm.

[23] S. Niyogi and E. Adelson, "Analyzing gait with spatiotemporal surfaces," In Proceedings of the IEEE Workshop Non-Rigid Motion, pages 24–29, Austin, November 1994.

[24] K. Delac and M. Grgic, "A survey of biometric recognition methods," In Proceedings of the 46th International Symposium Electronics in Marine (ELMAR-2004), pages 184–193, Croatia, June 2004.

[25] A. Muron and J. Pospisil, "The human iris structure and its usages," Acta Univ. Palacki, Phisica, vol. 39, pages 87–95, March 2000.

[26] John Daugman. Iris recognition, 2006. http://www.cl.cam.ac.uk/_jgd1000/.

[27] D. Gabor, "Theory of communication," *J. Inst. Electr. Eng.*, vol. 93, pp. 429–457, 1946.

[28] Karen Hollingsworth. SOURCES OF ERROR IN IRIS BIOMETRICS. M.S. thesis, University of Notre Dame, April 2008.

[29] L. Ma, T. Tan, Y. Wang and D. Zhang, “Efficient iris recognition by characterizing key local variations,” *IEEE Transactions on Image Processing* 13, 739–750, Jun. 2004.

[30] R. Wildes , "Iris recognition An emerging biometric technology," Proceedings of the IEEE, 85(9):1348–1363, September 1997.

[31] J. Cui, Y. Wang, T. Tan, L. Ma, and Z. Sun, "A fast and robust iris localization method based on texture segmentation," In Proceedings of the SPIE Defense and Security Symposium, vol. 5404, pages 401–408, August 2004.

[32] J. Huang, Y. Wang, Ti Tan, and J. Cui, "A new iris segmentation method for recognition," In Proceedings of the 17th International Conference on Pattern Recognition (ICPR04), vol. 3, pages 23–26, 2004.

[33] W. K Kong and D. Zhang, "Accurate iris segmentation method based on novel reflection and eyelash detection model," In Proceedings of the 2001 International Symposium on Inteligent Multimedia, Video and Speech Processing, pages 263–266, Hong Kong, May 2001.

[34] L. Ma, Y. Wang, and T. Tan, "Iris recognition using circular symmetric filters," In Proceedings of the 25th International Conference on Pattern Recognition (ICPR02), vol. 2, pages 414–417, Quebec, August 2002.

[35] Y. Zhu, T. Tan, and Y. Wang, "Biometric personal identification based on iris patterns," in *Proc. Int. Conf. Pattern Recognition*, vol. II, 2000, pp. 805–808.

[36] L. Ma, Y. Wang, and T. Tan, “Iris recognition based on multichannel Gabor filtering,” in *Proc. 5th Asian Conf. Computer Vision*, vol. I, pp. 279–283. 2002

[37] A. Ross and S. Shah, “Segmenting Non-Ideal Irises Using Geodesic Active Contours,” Proc. IEEE 2006 Biometric Symp., pp. 1-6, 2006.

[38] R. Donida Labati, V. Piuri, and F. Scotti, “Agent-Based Image Iris Segmentation and MultipleViews Boundary Refining”, in IEEE Third International Conference on Biometrics: Theory, Applications and Systems, November 20, 2009.

[39] Chen, Y., Adjouadi, M., Han, CA, Wang, J., Barreto, A., Rishe, N., and Andrian, J. "A highly accurate and computationally efficient approach for unconstrained iris segmentation," IMAGE AND VISION COMPUTING, p. 261, vol. 28, (2010).

[40] M. Vatsa, R. Singh, and A. Noore, “Improving Iris Recognition Performance Using Segmentation, Quality Enhancement, Match Score Fusion, and Indexing,” IEEE Trans. Systems, Man, and Cybernetics—Part B: Cybernetics, vol. 38, no. 4, pp. 1021-1035, Aug. 2008.

[41] H. Proenc¸a and L.A. Alexandre, “Iris Segmentation Methodology for Non-Cooperative Iris Recognition,” Proc. IEE Vision, Image, & Signal Processing, vol. 153, no. 2, pp. 199-205, 2006.

[42] X. Liu, K.W. Bowyer, and P.J. Flynn, “Experiments with an Improved Iris Segmentation Algorithm,” Proc. Fourth IEEE Workshop Automatic Identification Advanced Technologies, pp. 118-123, Oct. 2005.

[43] M. Dobes, J. Martineka, D.S.Z. Dobes, and J. Pospisil, “Human Eye Localization Using the Modified Hough Transform,” Optik, vol. 117, pp. 468-473, 2006.

[44] S. Schuckers, N. Schmid, A. Abhyankar, V. Dorairaj, C. Boyce, and L. Hornak, “On Techniques for Angle Compensation in Nonideal Iris Recognition,” IEEE Trans. Systems, Man, and Cybernetics-Part B: Cybernetics, vol. 37, no. 5, pp. 1176-1190, Oct. 2007.

[45] T. Tan, Z. He, and Z. Sun, "Efficient and Robust Segmentation of Noisy Iris Images for Non-cooperative Iris Recognition," *Image and Vision Computing (IVC)*, Vol.28, pp.223-230, 2010.

[46] J. Zuo, N. Kalka, and N. Schmid, "A Robust Iris Segmentation Procedure for Unconstrained Subject Presentation," Proc. Biometric Consortium Conf., pp. 1-6, 2006.

[47] http://www.griaulebiomertrics.com/page/understanding-biometrics/evaluation/

[48] T.A. Camus and R. Wildes, "Reliable and fast eye finding in close-up images," In Proceedings of the IEEE 16th International Conference on Pattern Recognition, pages 389–394, Quebec, August 2002.

[49] P. V. C. Hough, “Method and means for recognizing complex patterns,” U.S. Patent 3 069 654, 1962.

[50] J. Illingworth and J. Kittler, “A survey of the Hough transform,” Computer Vision Graph. Image Processing, vol. 44, pp. 87–116, 1988.

[51] H. Proença; "Iris Recognition: On the Segmentation of Degraded Images Acquired in the Visible Wavelength," IEEE Transactions on Pattern Analysis and Machine Intelligence, volume 32, number 8, pag. 1502-1516. August, 2010

[52] K. Hollingsworth, K. W. Bowyer and P. J. Flynn, "Pupil dilation degrades iris biometric performance," Comp.Vis. and Im. Understanding 113, no. 1, pp. 150-157, 2009

[53] X. Yuan, P. Shi, "A non-linear normalization model for iris recognition," In: Advances in Biometric Person Authentication, pp. 135–141 (2005)

[54] H. Wyatt, "A 'minimum-wear-and-tear' meshwork for the iris," Vision Research 40, 2167–2176 (2000)

[55] Z. Wei, T. Tan, and Z. Sun, "Nonlinear iris deformation correction based on Gaussian model," In Springer LNCS 4642: Int. Conf. on Biometrics, pages 780–789, Aug 2007.

[56] K P. Hollingsworth, K W. Bowyer, and P. J. Flynn, "The best bits in an iris code," IEEE Transactions on Pattern Analysis and Machine Intelligence, 31(6):964–973, Jun 2009.

[57] S. Ring and K. W. Bowyer, "Detection of Iris Texture Distortions By Analyzing Iris Code Matching Results," Biometrics: Theory, Applications and Systems (BTAS 08), September 2008, Washington, DC

[58] G. Dozier, D. Bell, L. Barnes, and K. Bryant, "Refining iris templates via weighted bit consistency," Proc. Midwest Artificial Intelligence and Cognitive Science (MAICS) Conference, pages 1–5, Apr 2009. Fort Wayne, Indiana.

[59] G. Dozier, K. Frederiksen, R. Meeks, M. Savvides, K. Bryant, D. Hopes, and T. Munemoto, "Minimizing the number of bits needed for iris recognition via bit inconsistency and grit," Proc. IEEE Workshop on Computational Intelligence in Biometrics: Theory, Algorithms, and Applications, pages 30–37, Apr 2009.

[60] D. Ballard, "Generalized Hough transform to detect arbitrary patterns," *IEEE Trans. Pattern Anal. Machine Intell.*, vol. PAMI-13, pp. 111–122,1981.

[61] Chester F. Carlson. Lecture 10: Hough circle transform. Rochester Institute of Technology: Lecture Notes, October 11, 2005.

[62] J. Canny. "A computational approach to edge detection," IEEE Transactions on Pattern Analysis and Machine Intelligence, vol. 8, pages 679–698, 1986.

[63] Anil K. Jain. Fundamentals of Digital Image Processing. Prentice-Hall International Editions, E.U.A., 1989.

[64] Gonzalez, Rafael C., R. E. Woods, and Steven L. Eddins. "Digital Image Processing using MATLAB," Prentice Hall, Upper Saddle River, NJ. 2004.

[65] H. Proença, L.A. Alexandre, "The NICE.I: noisy iris challenge evaluation part I," in: Proceedings of the of First International Conference on Biometrics: Theory, Applications, and Systems, 2007, pp. 1–4.

[66] Multimedia University. MMU iris image database, 2004. http://pesona.mmu.edu.my/ccteo.

[67] National Institute of Standards and Technology. Iris challenge evaluation, 2006. http://iris.nist.gov/ICE/.

[68] Michal Dobes and Libor Machala. UPOL iris image database, 2004. http://phoenix.inf.upol.cz/iris/.

[69] Institute of Automation, Chinese Academy of Sciences. CASIA iris image database, 2004. http://www.sinobiometrics.com.

[70] H. Proenc¸a and L. A. Alexandre, "UBIRIS: A noisy iris image database," In Proceedings of the 13th International Conference on Image Analysis and Processing (ICIAP2005), pages 970–977, Calgary, September 2005. http://iris.di.ubi.pt.

[71] L. Masek and P. Kovesi. MATLAB source code for a biometric identification system based on iris patterns. The University of Western Australia, 2003. http://www.csse.uwa.edu.au/~pk/studentprojects/libor/.

[72] J. Daugman, "New methods in iris recognition," IEEE Transactions on Systems, Man and Cybernetics - B, 37(5):1167–1175, Oct 2007

[73] M. Vatsa, R. Singh, and A. Noore, "Improving Iris Recognition Performance Using Segmentation, Quality Enhancement, Match Score Fusion, and Indexing", presented at IEEE Transactions on Systems, Man, and Cybernetics, Part B, 2008, pp.1021-1035.

[74] R. Wildes, J. Asmuth, G. Green, S. Hsu, R. Kolczynski, J. Matey and S. McBride. "A system for automated iris recognition," *Proceedings IEEE Workshop on Applications of Computer Vision*, Sarasota, FL, pp. 121-128, 1994.

[75] D. Field. Relations between the statistics of natural images and the response properties of cortical cells. *Journal of the Optical Society of America*, 1987.

[76] J. Thornton, M. Savvides, and B. Kumar, "A Baysian approach to deformed pattern matching of images," IEEE Transactions on Pattern Analysis and Machine Intelligence, 29(4):596–606, April 2007.